Journal of Archaeological Science: Reports 69 (2026) 105494

Contents lists available at ScienceDirect

Journal of Archaeological Science: Reports

journal homepage: www.elsevier.com/locate/jasrep

Provenance and technology of relief and/or lustre glazed ceramics from *Mértola* (Portugal)☆

Stamatina Nikologianni [a,e], José Mirao [a,b], Susana Gómez Martínez [b,c,d], Nicola Schiavon [a,b], Luis Dias [a,b], Helena Catarino [d], Elena Salinas [f], Massimo Beltrame [a,b,*]

[a] *Laboratório HERCULES, Évora University, Largo Marquês de Marialva n.° 8, 7000-809 Évora, Portugal*
[b] *Associated Laboratory In2Past, Largo Marquês de Marialva n.° 8, 7000-809 Évora, Portugal*
[c] *Campo Arqueológico de Mértola, R. António José de Almeida n.° 1-3, 7750-353 Mértola, Portugal*
[d] *CEAAPP, University of Coimbra, Colégio de S. Jerónimo, 1° Piso, Largo D. Dinis, 3000-395 Coimbra, Portugal*
[e] *National Centre for Scientific Research "Demokritos", Institute of Nanoscience and Nanotechnology, Aghia Paraskevi, 15341 Athens, Greece*
[f] *Escuela de Estudios Árabes, Consejo Superior de Investigaciones Científicas, Cuesta del Chapiz n.° 22, 18010 Granada, Spain*

ARTICLE INFO

Keywords:
Islamic period
Glazed pottery production
Lustreware
Provenance

ABSTRACT

This paper presents a study of a selection of lustre, relief, and lustre-relief glazed ceramics found at *Mértola* (12th–13th centuries), and *Coimbra* (11th century), Portugal (i.e. *Garb al-Andalus* during the Islamic period). The primary aim is to examine the possibility of a local production of lustre, relief, and lustre-relief wares at *Mértola*, and to compare the ceramic, glaze, and lustre technology employed with that applied in the production of lustre ceramics recovered at *Coimbra*, supposedly produced at Seville (Spain) during the 11th century. The analytical protocol included Optical Microscopy, X-ray Diffraction (XRD), X-ray Fluorescence (XRF), and Scanning Electron Microscopy coupled with Energy Dispersive Spectroscopy (SEM-EDS), in addition to High-Resolution Field Emission Gun Scanning Electron Microscopy (FEG-SEM). Considering the characteristics of the *Mértola* samples, during the 12th–13th centuries, different types of glazed ware, including lustre, relief, and lustre-relief, were locally produced, while others were imported. Conversely, *Coimbra* lustrewares evidenced significant technological differences, linking these samples to the Middle East tradition. To conclude, the results of this study evidenced, unexpectedly, that during the 11th century lustreware ceramics were imported into the *al-Andalus*, and not produced at Seville. The production started later, and *Mértola* ceramics from the 12th–13th centuries represent one ascertain example.

1. Introduction

Islamic glazed ceramics have been found across *al-Andalus* (the Iberian Peninsula during the Islamic Middle Ages), first imported and later produced locally (Salinas et al., 2018). Technologically, ceramic glaze is a glass layer applied to the ceramic surface, integrating with it through the firing process. Different glaze types existed in history, depending on the raw materials employed. The main component is silica (SiO_2), and different fluxing agents could be employed, such as lead (PbO) or alkali oxides (K_2O, Na_2O) (Tite et al., 1998). Glazes could be transparent or opacified using materials such as tin oxide (SnO_2), bone ashes, quartz grains, or eventually air bubbles (Mason & Tite, 1997; Salinas et al., 2017; Salinas & Pradell, 2024).

Regarding the Iberian Peninsula, the earliest production workshop of glazed ceramics in *al-Andalus* was found at *Pechina* (Salinas et al., 2019). At the workshop, galena (PbS) was roasted in open air at high temperature, and converted into lead oxide (PbO). The resulting oxide was then mixed with silica and subjected to a complex fritting process involving multiple stages of sand mixing, firing/melting/cooling, and crushing stages to obtain a homogeneous mixture (i.e. frit). The final glass was subsequently ground and applied to biscuit-fired ceramic bodies, which underwent a second firing stage to soften the obtained mixture and allow the adhesion of the resulting glaze to the vessel's surface.

In the 8th century CE, tin oxide (SnO_2) started to be employed in Islamic glazed ceramic production. It was employed for the production of yellow opaque glazes decorated with green and brown designs, firstly

☆ This article is part of a special issue entitled: '8th ARCH_RNT Proceedings - Archaeomaterials' published in Journal of Archaeological Science: Reports.

* Corresponding author at: Laboratório HERCULES, Évora University, Largo Marquês de Marialva n.° 8, 7000-809 Évora, Portugal.
E-mail address: massimo@uevora.pt (M. Beltrame).

https://doi.org/10.1016/j.jasrep.2025.105494
Received 29 July 2025; Received in revised form 4 November 2025; Accepted 12 November 2025

in Egypt (Coptic Glazed Wares) and then in Syria (Yellow Glaze Family Wares) (Tite et al., 2015; Matin, 2018). One century later, tin oxide was employed to create opaque white glazes in Abbasid Iraq (Tite et al., 2015), probably to imitate Chinese stoneware and porcelain (Matin, 2018; Tite et al., 2015; Ting et al., 2025; Wood et al, 2007; Zhao, 2013) Afterwards, the tin "technology" spread in the Islamic world, and it became a standard glazing technology in Islamic glazed pottery production, including in the production of metallic lustre glazed ceramics in Iraq, Iran, Syria, Egypt, and, eventually, in the Iberian Peninsula (Matin et al., 2018; Salinas & Pradell, 2020a; Pradell et al., 2008a; Pradell et al., 2013; Pradell et al., 2008b; Gutierrez et al., 2010).

Technologically, lustre is a nanosized metallic-glass composite embedded within a glassy matrix. It is formed by applying a raw metallic paint onto a previously glazed ceramic surface and then firing it again (Pradell et al., 2008b; Pradell & Molera, 2020). The production of the lustre layer involves a complex process driven by an ionic exchange between alkali ions from the glaze and silver and copper ions in the applied paint (Pradell & Molera, 2020). This exchange requires firing at relatively low temperatures, typically between 500 °C and 600 °C (Pradell et al., 2008b).

The resulting lustre layer can range in thickness from approximately 100 nm to 1 μm, with embedded metallic nanoparticles typically between 5 and 50 nm in size (Pradell et al., 2008b). The final colour of the lustre depends on the copper-to-silver (Cu/Ag) ratio: silver-rich lustres tend to appear yellow or green with golden tones, while copper-rich lustres exhibit amber, brown, or red hues (Pradell et al., 2008a). Another key factor influencing the lustre colour is the size of nanoparticles. Specifically, the size of the silver nanoparticles plays a significant role in determining the final colour. Smaller nanoparticles, typically around 10 nm in diameter, absorb shorter wavelengths of light, producing cooler hues such as green or blue. As the nanoparticle size increases, for example, to around 50 nm, the particles begin to absorb longer wavelengths, resulting in warmer tones such as yellow or gold. In addition to silver nanoparticles, the presence of copper in the lustre can further affect the final colour. Copper is typically found in the form of Cu^{+} or Cu^{2+} ions. The copper content promotes the growth of larger silver nanoparticles, with those pieces containing more copper tending to have larger silver particles (Pradell, 2016).

The distinctive metallic shine of lustre ceramics is primarily influenced by the diffusion of metallic ions within the glass substrate. A dense nanoparticulate layer—essential to produce a metallic shine—forms only when lead oxide (PbO) is present in the glaze. PbO reduces ionic mobility, promoting the formation of more concentrated and uniform metallic layers (Molera et al., 2007). In contrast, glazes with low lead content do not produce the characteristic metallic shine (Pradell et al., 2008c; Caiger-Smith, 1991; Carboni, 2001).

The first evidence of lustre decoration on pottery was discovered in the Caliphs' palace at *Samarra* (Iraq) and is believed to have been produced during the reign of Harun al-Rashid at the end of the 8th century (Pradell et al., 2007). According to Mason (2004), the first dedicated workshop for lustreware ceramics was established in *Basra* (Iraq), operating until the decline of the Abbasid dynasty in the late 10th century. Workshops were also active in *Fustat* (Egypt) during the Fatimid dynasty (10th–12th centuries), as well as in Syria, particularly in *Tell Minis* and *Raqqa*, during the 12th century. In Iran, lustre production is thought to have begun shortly after the fall of the Fatimid dynasty (Watson, 1985). The earliest Persian lustre piece is from 1179 CE, resembling Fatimid designs. This was followed by the Miniature style with smaller, more intricate designs, eventually evolving into the high-quality, standardised Kashan style of the early 13th century, characterised by thick lustre paint on a stonepaste body with tin-opacified glaze and dark-brown-golden colour. These centres developed diverse lustreware techniques, shaped by the cultural exchange and artisans' dislocations across different regions (Pradell et al., 2008b; Mason, 2004; Garofano et al., 2015; Pradell et al., 2013; Pradell et al., 2008a).

Lustreware ceramics were also imported into the Iberian Peninsula. Fifty-six examples of Samarra-type lustreware, finely made Islamic ceramics developed in 9th century Iraq, characterized by opaque white glazes (Matin et al., 2018), have been excavated in the palatial city of *Madinat al-Zahra* (Spain). These pieces date back to the 10th century, when they were imported from Tulunid Egypt, likely made by immigrant potters who introduced the Samarra ceramic tradition there (Heidenreich, 2012). The lustre technology finally reached the Iberian Peninsula around the middle of the 11th century (Pradell & Molera, 2020).

Scholars have suggested that the earliest lustreware workshops in the Iberian Peninsula were located in the *Taifa* Kingdom of *Seville* (Spain), under the control of the Abbadid dynasty (Barceló & Heidenreich, 2014). This production shows striking typological and stylistic similarities with Fatimid lustreware ceramic productions from *Cairo*, Egypt, suggesting that skilled Egyptian artisans migrated to *al-Andalus* to produce lustreware ceramics for the Abbadid rulers at *Seville* (Heidenreich, 2012). However, no lustreware ceramic workshops have been found to date, and similar lustreware ceramic fragments were analysed by Garofano et al. (2015), suggesting that ceramics were not locally produced but were imported from the Middle East.

Conversely, production sites have been identified at *Málaga*, Spain, during the mid-13th century, and in *Paterna* and *Manises*, Spain, during the first half of the 14th century (Gómez Moreno Martínez, 1924; Gómez-Martínez, 2006), as well as in *Zaragoza* and *Albarracín* during the mid-11th century during the *Taifa* Kingdom period. At *Almeria* (Spain), indications of metallic lustre relief ware ceramics production from the late 11th to 13th centuries have also been found, likely beginning during the Almoravid and continuing through the Almohad periods (Flores Escobosa & Navarro Ortega, 2012).

Moreover, seven lustreware fragments recovered at *Calatrava la Vieja* (Spain), dated from the end of the 12th to the beginning of the 13th centuries during the Almohad period, subjected to petrographic analysis, were found to match the geology of the region, indicating the existence of a local production (Zozaya et al., 1995). The same analytical approach was also applied to the study of lustreware (including relief ware) ceramics recovered at *Mértola* (Portugal), suggesting a local production also at this place during the 12th to the beginning of the 13th centuries (Zozaya & Aparicio, 2003). Finally, different scholars (Rosser-Owen, 2012; Heidenreich, 2012) indicated that during the second half of the 12th century, Almohad metallic lustre relief ware ceramics from *al-Andalus* were also exported to *Fustat* and *Cairo* (Egypt).

Consequently, lustreware ceramics from the Iberian Peninsula reflect not only the introduction of a new technology from the eastern Mediterranean but also the subsequent diffusion of these ceramics back into the same area centuries later. However, the precise timing and origin of these developments remain a matter of debate among specialists.

In Portugal, the biggest ceramic assemblage of lustre-decorated ceramics (from the 12th to 13th centuries) has been found at *Mértola* (Gómez Martínez, 2016; Gómez-Martínez, 2005; Gómez-Martínez, 1997). The town port of *Mértola* is located in the northernmost navigable limit of the river Guadiana and is considered by archaeologists, at least since the pre-Roman period, an intersection trade location point between the region, the European Atlantic coast, and the Mediterranean area (Gómez Martínez, 2016; Gómez-Martínez, 2003; Gómez-Martínez, 2006). But what was produced in the town? What was exported/imported? In this framework, ceramics represent a key material that can open a new window to the past. Different archaeological excavations have uncovered evidence of Islamic ceramic production at *Mértola* (Gómez Martínez, 2016; Gómez-Martínez, 2003), though none have been directly linked to the production of lustre, relief, and lustre-relief Islamic glazed wares. Thus, developing an integrated analytical approach is essential to determine ceramic characteristics, production technology, and provenance.

Common wares recovered at *Mértola* from productive contexts will be used as "standard" of the locally available raw material and compared with other common wares, relief and lustrewares from the same town to

speculate about ceramic provenance and technology applied. Moreover, lustreware ceramics recovered at *Coimbra* (Fig. 1), Portugal, dating back to the 11th century, have been included in this study. *Coimbra* ceramic samples show striking similarities with *Seville* lustreware ceramic specimens. Thus, the ceramic, glaze, and lustre technology between the two cities can be compared. Ultimately, the aim of this paper is to assess the likelihood of a relief and lustreware workshop having operated in the area of *Mértola*. Thanks to the analysis of *Coimbra* samples, it will also be possible to collect information about the introduction of lustre technology in *al-Andalus*, its evolution, and diffusion. These questions will be addressed using a range of optical and analytical methods, namely optical microscopy (OM), X-ray diffraction (XRD), and X-ray fluorescence (XRF). In addition, scanning electron microscopy (SEM) coupled with an energy dispersive spectrometer (EDS) will provide insights into ceramic paste microstructure, glaze, and lustre characteristics.

2. Geological setting of the region of *Mértola*

From a geological point of view, *Mértola* is located in the southeast of Portugal and belongs to the South Portuguese Zone (SPZ). SPZ is located in the southernmost portion of the Iberian Variscan Massif, whose rocks are representative of the Iberian Pyrite Belt, an area known for metal enrichment zones formed through hydrothermal alteration (Almodóvar et al., 2019). Three main lithostratigraphic units (Fig. 2) of sedimentary and igneous rocks from the Upper Palaeozoic (Givetian–Visean) make up the stratigraphic sequence of the SPZ. These are the Phyllite/Slate-Quartzite Group (PQ Group), the Volcano-Sedimentary Complex (VSC), and the Low *Alentejo* Flysch group (i.e. a thick post-volcanic turbiditic succession). Each unit's stratigraphic boundaries are depositional, and the whole stratigraphic sequence can be easily recognised at the Pomarão Geosite (https://geossitios.progeo.pt/geosites/corte-geologico-do-pomarao). Phyllites dominate the PQ group, with fine-grained quartzite and siltstones piled on top of it. Conglomerates, greywacke, lenses of jasper can be found, in addition to dark phyllite with intervening nodules and metric/decametric lenticular beds of carbonate rocks. Mafic and felsic igneous rocks, siltstone, jaspers, and cherts, as well as slates rich in clay and quartz, represent the VSC complex. The various lithologies manifest as variably extended lenticular outcrops. In this area, the Low *Alentejo* Flysch is referred to as the *Mértola* Formation (MT). It is a sequence of bedded turbidites (i.e., greywackes) and pelitic deposits (i.e., slates) (Camara et al., 2023; Beltrame et al., 2022; Schermerhorn, 1971; Oliveira and Silva, 2007).

Fig. 1. Map of the Iberian Peninsula showing the location of the three cities from which the analysed material originates.

3. Materials and methods

3.1. Materials

Islamic ceramics included in this study (Fig. 3, Table 1) were recovered in two different Portuguese cities (Fig. 1), namely *Mértola* and *Coimbra*. The largest assemblage, from *Mértola*, includes eight decorated and six common ware samples. The *Coimbra* samples consist of two lustreware ceramics.

The metallic lustre ceramic samples from *Coimbra* are part of the collection of CEAAPP, University of *Coimbra.* These two fragments were recovered during excavations at the courtyard of the University of Coimbra (Portugal), found within a palatial context associated with the *alcaçova da Madinat Qulumbriya*. They are the only lustreware pieces recovered in the area (Catarino et al., 2009). Sample COI1 is a fragment of a small bowl with a slightly broken profile and a flat lip. The internal decoration shows an epigraphic motif between cartouches surrounding the lip. In contrast, the external decoration features a set of tiny dots, some positioned between thin stroke cartouches, which limit the lower part of the lip and the beginning of the body, while others are located on the outside and in the centre of circles, also featuring thin strokes. Sample COI2 is a fragment of the lip of a bowl, which is slightly flared. The external decoration shows a band near the lip and traces of undetermined motifs, and the internal epigraphic motif, limited by a band near the lip, presents part of an inscription, where the name "Almutamid?" (*Abbadid* prince of the *Taifa* Kingdom of *Sevilla*) can be inferred (Catarino et al., 2009; Barceló & Heidenreich, 2014). Both samples exhibit a brown and amber lustre, lacking a metallic shine. They differ significantly from those previously identified in the *Gharb al-Andalus* (western part of the Iberian Peninsula) region, as their profiles, decorations, and dimensions do not resemble known Almoravid or Almohad lustreware ceramics. According to Catarino et al. (2009), this suggests they may be eastern imports or early examples of lustreware production, possibly originating in *Seville*.

The ceramic samples from Mértola are part of the collection of *Campo Arqueológico de Mértola.* A total of 43 different vessels with lustre decorations have been recovered from different archaeological excavations in the area, almost all incomplete, some of which consist of only one or two fragments (Gómez-Martínez, 1997; Gómez-Martínez, 2006). The samples used in this study span the 12th to 13th centuries, corresponding to the *Almohad* occupation of the town (Gómez-Martínez, 1997, 2005, 2014). Two common ware ceramic samples, from the 10th–11th century, were also included to assess the continuity in raw material exploitation during the Islamic period of the town's occupation.

Sample MER1 is a fragment of a small bottle (i.e. *garrafa*), with a vertical triangular rim, an extremely small neck, a piriform body, and a flat circular base. It is covered by a monochromatic honey-brown coloured glaze on the outer surface, undecorated on the inside. Samples MER 2, 3, 6, and 7 are jars, classified as "relief wares" (Barceló & Heidenreich, 2014), produced using bivalve moulds, showing metallic lustre decoration or not. Typologically, these jars show a high neck shaped like a truncated inverted cone, a globular body, a vertical handle (when present), a convex base, and a ring foot inclined outward. The outside decorative pattern is mainly composed of vegetal motifs. They are believed to have been produced using the same/similar moulds, just changing the glaze colour or lustre appearance on the outer surface of the jar (Gómez-Martínez, 2005; Gómez Martínez, 2014). Similar vessels have been found at the cities of *Fustat* and *Cairo,* in Egypt, at *Cordoba*, *Málaga*, *Almería*, *Jerez de la Frontera* in Spain (Martínez Cabiró, 1975; Gómez Moreno Martínez, 1940; Duda, 1970; Fernández Gabaldón, 1987) and at the Portuguese cities of *Silves* and *Alcaçer do Sal* (Varela Gomes, 1991; Paixão et al., 2001). Evidence of production has been discovered at *Almeria*, in Spain (Flores Escobosa & Navarro Ortega, 2012).

Sample MER4 is a fragment of a bowl with a rounded, straight rim

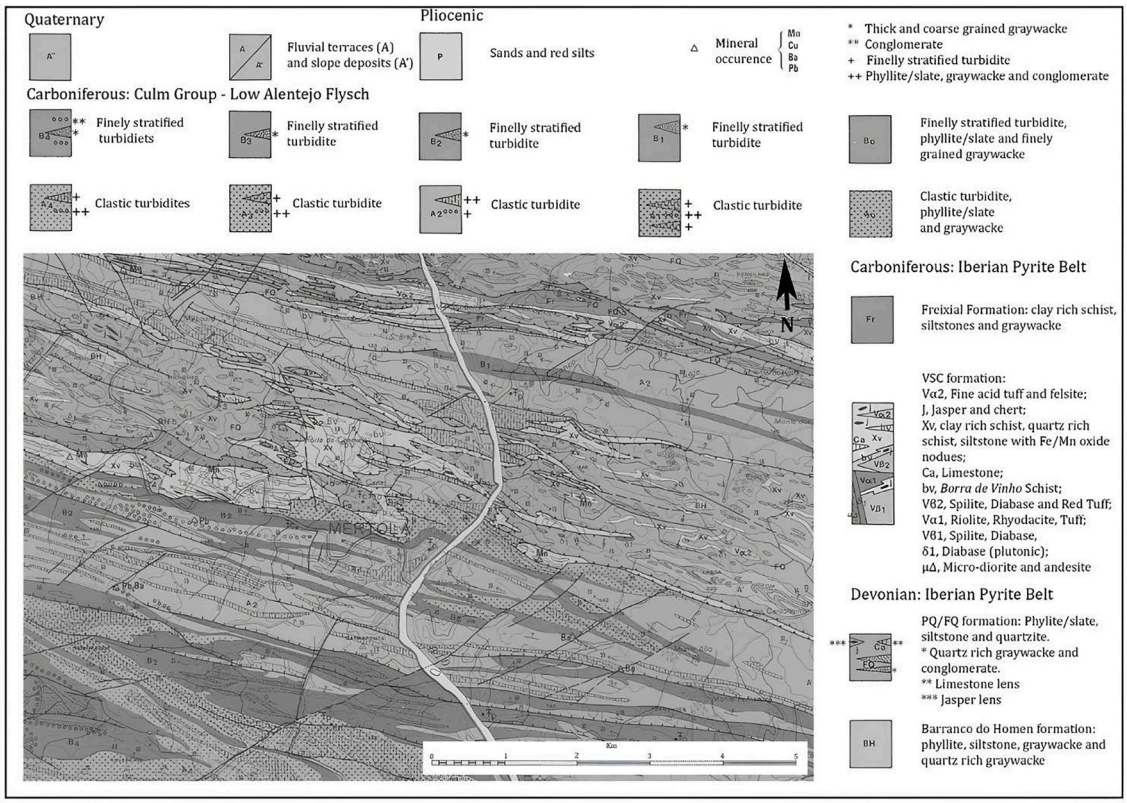

Fig. 2. Simplified Mértola region geological map (adapted by Beltrame et al., 2022, from Oliveira and Silva, 1990).

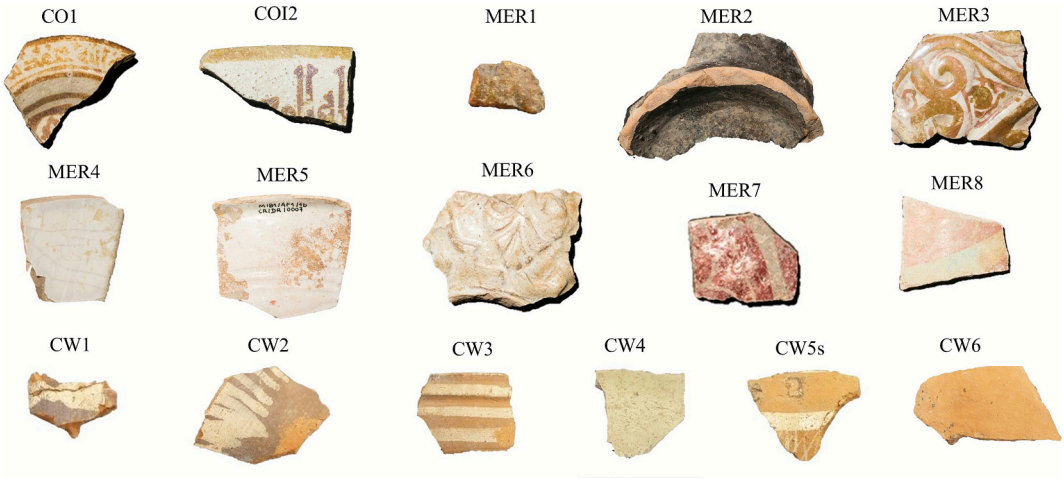

Fig. 3. Pictures of all the samples included in this study, with their assigned name.

and hemispheric body. The lustre decoration on the white glaze can be barely seen, close to the rim, on both the inside and outside of the bowl. On the interior side, epigraphic and vegetal motifs are included within two concentric bands. The decorative patterns show striking similarities with pieces recovered at *Granada*, *Palma de Mallorca*, *Malaga*, and at *Cova dels Amagatals* (Gómez-Martínez, 1997; Gómez Martínez, 2014). Sample MER5 is also a fragment of a bowl with an outwardly flared rim and hemispheric body. The decoration is similar to MER4, but it is composed solely of concentric bands near the rim (Gómez-Martínez, 1997). Finally, sample MER8 is a fragment of a jar with metallic lustre decoration on the outer surface and glaze on the inner.

Two common ware samples (CW1 and CW2) were discovered in a kiln context (Gómez-Martínez, 2014) and will, therefore, serve as standards for the locally exploited raw material used in ceramic production. Samples CW3 and CW4 were recovered in a cryptoportico in *Alcáçova do Castelo de Mértola* and samples CW5 and CW6 were recovered in a pit in the excavation of the *Castelo de Mértola*. Sample CW1 is a fragment of a small jar with white decoration on top of a dark-coloured slip on the outer surface. CW2 is a fragment of an unidentified vessel type, recovered from a kiln context as well. On the exterior, it features a white-painted decoration on the vessel's neck. CW3 is a fragment of a pot with white painted decoration of 3 parallel horizontal lines on the outer surface of the vessel. Sample CW4 is a fragment of a jar decorated with red paint. Sample CW5 is a fragment of a small jar with a white, coloured painted decoration of a horizontal band featuring a reticular motif on the exterior surface of the body. Finally, sample CW6 is a

Table 1
List of the samples indicating the reference number, the code name used in the study, location, typology, decoration, and relative chronology. For most of the samples from Mértola, the catalogue number and pages are provided (Gómez-Martínez, 2014).

Sample Arch Ref.	Lab. Code	City/ Town	Typology	Paste colour	Glaze inside	Glaze outside	Decoration	Century	Lustre	Lustre colour	Metallic Shine	Reference
IAPUC2002UE20-20-	COI1	*Coimbra*	Bowl	Pinkish	White, opaque	White, opaque	Metallic lustre	Mid 11th	Yes	Amber and Brown	No	Catarino et al. (2009), fig. 19, pp 378
IAPUC2001UE57-6-	COI2	*Coimbra*	Bowl	Beige	White, opaque	White, opaque	Metallic lustre	Mid 11th	Yes	Amber and Brown	No	Catarino et al. (2009), fig. 19, pp 378
CR/VC/0025	MER1	*Mértola*	Jar	Red	No	Honey-Brown, transparent	Glaze	Second half 12th – First half 13th	No	No	–	Gómez Martínez, (2014), 260, p.414
CR/DR/0023	MER2	*Mértola*	Jar	Red	Honey-coloured, transparent	Black, opaque	Relief ware	Second half 12th	No	No	–	Gómez Martínez, (2014), 185, p.389
CR/DR/0002	MER3	*Mértola*	Jar	Red	Honey-colored	White, opaque	Relief ware with metallic lustre	Second half 12th	Yes	Golden	Yes	Gómez Martínez, (2014), 181, p.388
CR/DR/0010	MER4	*Mértola*	Bowl	Red	White, opaque	White, opaque	Metallic lustre	End of the 12th – beginning of the 13th	Yes	Golden	Weathered	Gómez Martínez, (2014), 153, p.378
CR/DR/0007	MER5	*Mértola*	Bowl	Red – Buffy	White, opaque	White, opaque	Metallic lustre	End of the 12th	Yes	Golden	Weathered	Gómez-Martínez, (1997), pp 150
M82/6C/3A181	MER6	*Mértola*	Jar	Buffy	Honey-coloured, transparent	White, opaque	Relief ware with metallic lustre	Second half 12th	Yes	Golden	No – Lost?	Gómez Martínez, (2014), 180, p.387
M 79 AC2 1B	MER7	*Mértola*	Jar	Red	Honey-coloured, transparent	White, opaque	Relief ware with metallic lustre	Second half 12th	Yes	Red	Yes	Not published
M/997/3B/1E	MER8	*Mértola*	Jar	Red	Honey-coloured, transparent	Green, transparent	Metallic lustre	Second half 12th	Yes	Red	Yes	Not published
R25 Abril (0009)	CW1	*Mértola – kiln*	Small jar	Brown-Red	No	No	White painted	Second half 12th – First half 13th	No	No	–	Gómez Martínez, (2014), p.270
No 114	CW2	*Mértola – kiln*	Unidentified	Brown-Red	No	No	White painted	Second half 12th – First half 13th	No	No	–	Gómez Martínez, (2014), p.270
CR/PT/0026	CW3	*Mértola*	Cooking pot	Brown	No	No	White painted	12th	No	No	–	Gómez-Martínez, (2006) p.1591
CR/BR/0026	CW4	*Mértola*	Jar	Buffy	No	No	Red painted	Second half 12th – First half 13th	No	No	–	Gómez Martínez, (2014), 191, p.391
CR/PT/0054	CW5	*Mértola*	Jar	Orang	No	No	White painted	10th/11th	No	No	–	Gómez Martínez, (2014), 172, p.385
CR/CC/0102	CW6	*Mértola*	Cooking pot	Orange	No	No	Engobe red decoration	10th/11th	No	No	–	Gómez-Martínez, (2006) p.904

fragment of a pot with engobe red decoration on the exterior surface.

3.2. Methods

Optical microscopy (OM) was developed on ceramic thin sections. In the case of Coimbra samples, thin sections were not prepared due to sampling restrictions. For the analysis of the thin sections, a Leica DM2500P transmitted light microscope equipped with a Leica MC 170HD digital camera for image capture was used. Thin-section ceramic characterisation, including temper percentage, roundness, and sorting, was performed following the scheme proposed by P. S. Quinn (2013).

To determine the mineralogical composition of the samples, X-ray diffraction (XRD) was employed. Apart from the powder XRD method (applied for most samples), micro-XRD (μXRD) was used in the case of *Coimbra* samples because of sampling restrictions. In these cases, five spots were analysed by micro-XRD for each sample, and results were joined in a single interpretation. The equipment used for all the samples is the Bruker AXS D8 Discover XRD with the Da Vinci design. A Cu Kα source operating at 40 kV and 40 mA and a Lynxeye 1-dimensional detector were used. Scans were run from 3 to 75° 2θ, with a 0.05 2θ step and 1 s/step measuring time by point. Interpretations were done using Diffrac Eva software, using the PDF2 database.

Major oxides and trace elements concentration were determined using a Bruker™ S2 Puma energy-dispersive XRF spectrometer (ED-XRF), equipped with a silver anode x-ray tube. The instrument was operated following a careful calibration routine using siliceous commercial standards (Beltrame et al., 2019; Beltrame et al., 2021; Camara et al., 2023; Camara et al., 2025). Data acquisition and processing were performed using Spectra Elements 2.0 software, resulting in a table displaying the concentration of major oxides and trace elements, including their associated instrumental statistical errors. Regarding sample preparation for XRF analyses, for each specimen, fine powders were prepared, except for the two samples from Coimbra. Decorated samples were also subjected to an additional procedure that involved removing the decoration from the surface using a drilling machine. After the preparation of powders, the analytical protocol requires the preparation of glass beads using a fusion machine. For this purpose, 12 g of flux (lithium tetraborate plus lithium iodide) were mixed with 1.2 g of each sample's fine powder. After being placed in a crucible, the mixture was fired in the fusion machine at 1065 ℃ for 24 min, forming a glass bead. Loss on ignition (LOI) was determined by calcination of roughly 1 g of each sample in a muffle furnace at 1065 ℃ for 30 min.

Microstructural and chemical analysis of samples, ceramic paste and glaze were developed using a HITACHI S3700N SEM coupled with a Quantax EDS microanalysis system equipped with a Bruker AXS XFlash® Silicon Drift Detector (129 eV Spectral Resolution at FWHM/MnKα). PhiRhoz quantitative elemental analysis was performed using the Bruker ESPRIT software. The operating conditions for EDS analysis were as follows: BSEM mode (BSEM), 20 kV accelerating voltage, 10 mm working distance, 120 μA emission current. The detection limits for major elements (>Na) were in the order of 0.1 wt% (Schiavon et al., 2015).

Lustre decorations were evaluated using a High-Resolution Field Emission Gun Scanning Electron Microscopy (FEG-SEM) coupled to an energy dispersive X-Ray spectrometer (EDS). Lustre layer thickness, nanoparticle size, and the chemical composition of the layer were determined. Sample resin blocks were carbon-coated before analysis. The instrument used was Field Emission Scanning Electron Microscopy (TESCAN Clara, Czech), operating under variable pressure 100–160 Pa – H_2O, at 20 kV accelerating voltage, 1 nA current, and 6–8 mm working distance. The detector used was the Everhart–Thornley secondary electron detector. The EDS experiments were performed with an X-ray spectrometer, Bruker XFlash 6130 SDD detector, with 126 eV spectral resolution at the FWHM/Mn Kα. Compositional data were acquired in the same conditions using the PhiRhoz quantitative analysis method. Data were treated using Espirit 2.5 software from Bruker.

4. Results and discussion

4.1. Optical Microscopy results

Thin sections from all samples (except the two samples from *Coimbra*) were examined and categorised into three fabrics (Fig. 4) based on the identification of minerals, rock fragments (Table 2), and matrix characteristics (Table 3). Thin-section ceramic characterisation, including temper percentage, roundness, and sorting, was performed following the scheme proposed by P. S. Quinn (2013). Temper classification was made according to the Wentworth grain size classification (Wentworth, 1922).

F1: It includes two samples, CW4 and MER6, recovered at *Mértola*. The samples have a buffy, homogeneous ceramic matrix. Paste's appearance indicates the utilisation of a calcium-rich clay for ceramic production (Fabbri et al., 2014). Additionally, unmixed clay pellets were observed. Porosity is low, and it is characterised by the presence of vesicles up to 100 μm. Temper, 5 % in total, consists of moderately sorted, rounded inclusions with high sphericity and a bimodal grain size distribution, with one group of inclusions measuring approximately 300 μm (medium sand) and the other measuring approximately 50 μm. (coarse silt). Temper alignment is weak-absent. Mineralogically, they are characterised by the presence of quartz (predominant), K-rich feldspars (moderate), and weathered biotite (rare). Regarding rock fragments, quartzite, schist, and phyllite were observed.

F2: It comprises CW1, CW2, CW3, CW5, CW6 and MER1 from *Mértola*. The matrix is non-calcareous, iron-rich and homogeneous in all cases. The colour is brown to reddish brown. The porosity is abundant and composed of vughs, planar voids, and vesicles up to 200 μm. Temper, around 40 % in total, consisted of moderately sorted, angular, with low sphericity inclusions that have both bimodal and unimodal distributions with a temper size ranging between 50 (coarse silt) and 800 μm (coarse sand) μm. Mineralogically, this fabric is characterised by quartz (predominant), potassium-rich feldspar (moderate), plagioclase (moderate), and muscovite crystals (rare). Rock fragments of quartzite, greywacke, and shale were observed.

F3: It comprises MER2, MER3, MER4, MER5, MER7, and MER8 from *Mértola*. The matrix is also in this case non-calcareous, iron-rich and homogenous with a reddish-brown to brown colour. Porosity is low and composed of vesicles up to 100 μm. Regarding temper, which accounts for approximately 10–30 % of the total, inclusions are mostly subangular with moderate to low sphericity. Most samples are moderately to well sorted, with two samples (MER2, MER4) exhibiting well-sorted inclusions. The grain size distribution is both unimodal (MER2, MER4, MER5) and bimodal (MER3, MER7, MER8). Sample temper size ranges between 10 (fine silt) and 200 μm (fine sand). Mineralogically, all samples contain quartz (predominant), K-rich feldspars, plagioclase (moderate), and muscovite (rare). Regarding rock fragments, greywacke, chert, and quartzite were observed.

Optical microscopy results provide preliminary insights into the ceramic's possible provenance and technology. First of all, OM results of CW1 and 2 evidenced that quartzite, phyllite, greywacke, and chert were common rock fragment inclusions, and the association with the local Phyllite/Slate-Quartzite Group (PQ Group) and Volcano-Sedimentary Formation (VSC) can be stated (i.e. section 2). Consequently, all samples included in F2 were produced at *Mértola*. Considering F2 samples' relative chronology, a continuity in the exploitation of the same raw material over time can also be confirmed. Samples included in the group F3 are very similar to F2 samples. Additionally, OM results indicate compatibility with the local geology, and the primary difference between F2 and F3 is represented by temper sorting and grain size. Thus, the raw material employed was very similar, but it was treated differently, and the ceramist extracted bigger temper grain, increasing the clay-to-temper ratio.

In the case of F1, the identified minerals and rock fragments are not compatible with the group F2, and consequently, with the local geology

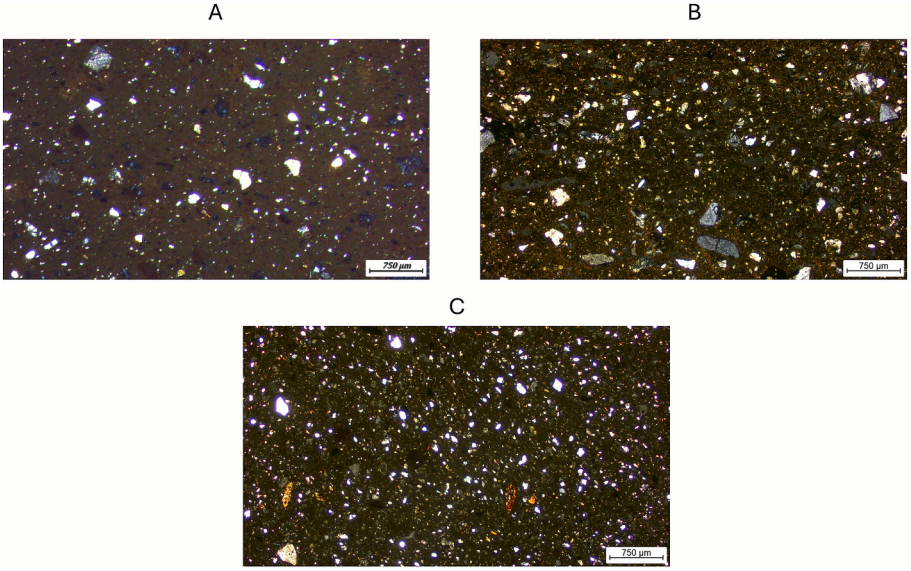

Fig. 4. A. A representative microphotograph (XPL) of the sample MER6 of PF1. B. A representative microphotograph (XPL) of the sample CW6 of PF2. C. A representative microphotograph (XPL) of the sample MER2 of PF3.

Table 2
Temper material description of the mineral, rock fragments and distinctive inclusion particulates identified by Optical Microscopy.

Group		Provenance	Typology	Mineralogy	Rock fragments	Observations
F1	CW4	*Mértola*	Jar	Quartz, K-rich feldspars, some biotite	Quartzite	Very poor in temper
	MER6	*Mértola*	Jar		Schist, phyllite, quartzite	Poor in temper
F2	CW1	*Mértola*	Small jar	Quartz, K-rich feldspars, some muscovite, plagioclase	Quartzite, greywacke, chert	Very rich in temper, clay pellets
	CW2	*Mértola*	Unidentified		Shale, quartzite, greywacke	Very rich in temper
	CW3	*Mértola*	Cooking pot		Shale, quartzite, greywacke	Very rich in temper
	CW5	*Mértola*	Jar		Quartzite, greywacke, chert, sandstone, granitic rock fragment	Very rich in temper
	CW6	*Mértola*	Cooking pot		Quartzite, greywacke, chert	Very rich in temper
	MER1	*Mértola*	Bottle		Quartzite, greywacke, chert, shale	One crystal was identified as amphibole.
F3	MER2	*Mértola*	Jar	Quartz, K-rich feldspars, plagioclase, muscovite	Fragments of greywacke, quartzite	
	MER3	*Mértola*	Jar		Fragments of greywacke, quartzite	
	MER4	*Mértola*	Bowl		Fragments of greywacke, quartzite	
	MER8	*Mértola*	Jar		Fragments of greywacke, quartzite	Poor in temper, lots of voids
	MER5	*Mértola*	Bowl		Fragments of greywacke, quartzite	Poor in temper, lots of voids
	MER7	*Mértola*	Jar		Fragments of greywacke, quartzite	

near the town of *Mértola*. Another difference is that F2 samples can be found in the ceramic paste. Besides its colour, it clearly suggests the exploitation of a pure carbonate-rich clay. At present, it is not possible to suggest a possible provenance, but similar raw materials are easily available in southern Iberia.

4.2. X-ray diffraction results

After XRD analyses, two different XRD groups (i.e. XRD groups 1 and 2) were identified. Unlike OM results, samples from different fabrics could be included in the same XRD group (Table 4).

XRD group 1 primarily consists of ceramics with glaze or lustre decorations, as well as one common ware. The group is generally characterised by the presence of quartz, feldspars, illite/muscovite, in addition to pyroxenes, gehlenite, and plagioclases (not identified in thin section). Minor mineralogical phases are represented by feldspathoids, hematite, and calcite. Thus, based on the mineralogical phases identified on XRD group 1, a calcium-rich raw material was employed in ceramic manufacturing. This is supported by the development of newly formed calcium-rich mineralogical phases, such as pyroxenes, gehlenite, and plagioclases, within the ceramic paste, which could not be observed or identified during optical microscopy (OM) analyses.

Regarding the firing technology applied on XRD group 1 samples, gehlenite starts nucleating around 800 °C from free lime after the decarbonation process of carbonates (Fabbri et al., 2014). Afterwards, gelhenite, being a metastable mineralogical phase, at temperatures above 1050 °C, reacts with the silica released by phyllosilicates decomposition to form anorthite and calcium-rich pyroxene (Heimann & Maggetti, 2019). Moreover, Illite/muscovite typically vanishes at firing temperatures exceeding 950 °C (Riccardi, 1999; Ouahabi et al., 2015; Nodari et al., 2007; Heimann & Maggetti, 1981; Rathossi et al., 2017). This is the case of the ceramic samples recovered at *Coimbra* and one sample recovered at *Mértola*. Thus, the firing temperature range of XRD group 1 can be estimated between 800 and 1050 °C, represented by the lower crystallisation limit of gelhenite and the upper decomposition limit of the same mineral. The simultaneous presence of calcite and gehlenite indicates that the calcite present in sample MER7 is, in fact, secondary calcite, probably from re-carbonation of free lime inside the ceramic paste or, eventually, by gehlenite alteration (Heimann & Maggetti, 1981; Rathossi et al., 2017; Fabbri et al., 2014). The identification of analcime can be attributed to a later contamination during burial (Ferreira et al., 2016).

XRD group 2 includes only common ware from *Mértola*. It is characterised by the presence of illite/muscovite, quartz, feldspars and

Table 3
Ceramic paste analysis (Grain size distribution (G.S.D.): unimodal, U; bimodal, B;Fabric, F – Matrix homogeneity/heterogeneity: Hom; Het;

Sample	Typology	Decoration	Colour	F	Ceramic paste %	Hom-Het	Temper	Roundness	Alignment	Sorting	G.S.D.
CW1	Small jar	White painted	Reddish brown	1	60 %	Hom	40 %	Moderately rounded with high sphericity	No	Moderately	B
CW2	Unidentified	White painted	Reddish brown	2	60 %	Hom	40 %	Angular with low sphericity	No	Moderately	B
CW3	Pot	White painted	Reddish brown	2	60 %	Hom	40 %	Angular with low sphericity	No	Moderately	B
CW4	Jar	Red painted	Buffy	1	90 %	Hom	10 %	Moderately rounded with high sphericity	No	Moderately	B
CW5	Jar	White painted	Reddish brown	2	60 %	Hom	40 %	Angular with low sphericity	No	Moderately	B
CW6	Pot	Engobe red decoration	Brown	2	60 %	Hom	40 %	Angular with low sphericity	No	Moderately	B
MER1	Bottle	Glaze	Reddish brown	2	60 %	Hom	40 %	Angular with low sphericity.	No	Moderately	B
MER2	Jar	Relief ware	Brown	3	70 %	Hom	30 %	Subangular, low sphericity	Poorly	Well shorted	U
MER3	Jar	Relief ware with metallic lustre	Brown	3	70 %	Hom	30 %	Subangular and low sphericity	Poorly	Moderately to well sorted	B
MER4	Bowl	Metallic lustre	Reddish brown	3	90 %	Hom	10 %	Subangular with moderate sphericity	Yes	Well sorted	U
MER5	Bowl	Metallic lustre	Reddish brown	3	90 %	Hom	10 %	Subangular with moderate sphericity	No	Moderately to well sorted	U
MER6	Jar	Relief ware with metallic lustre	Buffy	3	90 %	Hom	10 %	Angular with low sphericity.	No	Moderately	U
MER7	Jar	Relief ware with metallic lustre	Brown	3	90 %	Hom	10 %	Subangular with moderate sphericity	Moderately	Moderately to well sorted	B
MER8	Jar	Metallic lustre	Reddish brown	3	90 %	Hom	10 %	Poorly rounded with low and high	No	Moderately to well sorted	B

hematite. Therefore, the raw material employed corresponded to a silica-rich raw material. The firing technology applied can be evaluated thanks to the identification (or not) of hematite, illite/muscovite, and mullite. The first one typically crystallises at 750 °C (Riccardi, 1999), illite/muscovite typically vanishes at firing temperatures exceeding 950 °C (Nodari et al., 2007; Heimann & Maggetti, 1981; Rathossi et al., 2017) and mullite generally crystallizes when the firing temperature exceeds 1000 °C (Ouahabi et al., 2015). Considering that hematite was consistently identified, illite/muscovite was not detected systematically, and mullite was never identified, the firing temperature range for XRD group 2 can be estimated between 750 and 1000 °C.

Considering XRD results, two different families of raw materials were chosen for the production of the ceramic samples included in this study. A silica-rich raw material was generally preferred for the production of common wares. This is the case of the most common ware samples included in F2. Nevertheless, a calcium-rich raw material could also be employed (see sample CW4 included in F1). This suggests that the raw material selection could be the result of its large availability close to the workshop. On the contrary, all decorated samples (including F1 and F3) were produced using a calcium-rich raw material. This result was expected, as it is the most diffuse technology employed for the production of glazed ceramics during the Islamic period (Tite et al., 1998). To this scheme, only one exception has been identified. This is represented by the sample MER1 (i.e. monochromatic glazed ceramic sample). Based on the results obtained during OM observation, the sample was initially included in the F2 group as it perfectly matched the characteristics identified in samples CW1 and CW2 retrieved in a ceramic production archaeological context at *Mértola*. Thus, XRD results confirm, as explained in section 2, the variability of the Phyllite/Slate-Quartzite Group (PQ Group).

4.3. SEM-EDS and XRF: Ceramic paste characteristics

The results obtained from SEM-EDS and XRF analyses were used to: a) examine the microstructure and chemical composition of the ceramic pastes, and b) assess similarities and/or differences in the chemical composition of the ceramic bodies.

The chemical composition of the ceramic bodies was determined using SEM-EDS by averaging three or more measurement points per sample, avoiding areas with temper, porosity, or visible inhomogeneities. Elemental concentrations were normalised to 100 % and converted to oxides. Results are reported as average values (AVR) with standard deviations (SD), expressed as oxides in wt% (weight percent). Due to the nature of the ceramic bodies, these measurements are considered semi-quantitative and not representative of the ceramics' bulk chemical composition. XRF analysis was conducted on all samples, except those recovered at *Coimbra*, due to sampling restrictions. Major elemental compositions are reported in weight percent (wt%), while minor and trace elements are expressed in parts per million (ppm).

All data obtained from SEM-EDS and XRF analyses are provided in the supplementary materials (see Supplementary Files: S1 and S2, respectively).

4.3.1. Combining SEM-EDS and XRF results: Supporting XRD results

The compositional data obtained by SEM-EDS and XRF analyses were initially used to corroborate XRD results. Chemical data were plotted into the $CaO + MgO$ vs Al_2O_3 vs SiO_2 system, which represents a forecast of the mineralogical composition that should develop at a temperature of 1100 °C under oxidising conditions (Heimann & Maggetti, 2019). The difference between applying the two methods is represented by "the scale of analysis". XRF is a bulk analysis; the sample is considered in its totality, including temper (Fig. 6). The application of SEM-EDS analysis (Fig. 5) to a restricted area of the ceramic paste eliminates the overestimation of SiO_2, which is highly concentrated in the temper and does not contribute to the crystallisation of high-temperature mineralogical phases.

Results revealed two clusters that support the OM and XRD findings. The chemical composition of XRD group 1 is consistent with the identification of high-temperature calcium-rich mineralogical phases plotting in the triangular space included between quartz, anorthite, wollastonite-diopside or inside the triangle anorthite, wollastonite-diopside, gehlenite (i.e. calcium-rich areas). Conversely, the XRD

Table 4
Semi-quantitative determination of the mineralogical phase's abundance identified by XRD. (Legend: tr, traces; x, scarce; xx, moderate; xxx, frequent; xxxx, abundant).

Place of recovery	Sample	Decoration	Analysis mode	Fabric	XRD group	Quartz	Pyroxenes	Gehlenite	Analcime	Potassium-rich feldspar	Hematite	Plagioclase	Illite/ muscovite	Calcite
Mértola	CW1	White painted	Powder	F2	Group 2	xxxx				x	tr	x		
	CW2	White painted	Powder	F2	Group 2	xxxx				x	tr	xx	xx	
	CW3	White painted	Powder	F2	Group 2	xxxx				xx	x			
	CW4	Red painted	Powder	F1	Group 1	xxxx	xxx	xxx	xx	x				
	CW5	White painted	Powder	F2	Group 2	xxxx				x	tr	x	x	
	CW6	Engobe red decoration	Powder	F2	Group 2	xxxx					tr	xx	x	
	MER1	Honey-brown glaze	Powder	F2	Group 1	xxxx	x	x		x	x	x	x	
	MER2	Relief ware	Powder	F3	Group 1	xxxx	x	x		x	x	xx	x	
	MER3	Relief ware with metallic lustre	Powder	F3	Group 1	xxxx	x	x			tr	xx	x	
	MER4	Metallic Lustre	Powder	F3	Group 1	xxxx	x	xx		x	x	x	x	x
	MER5	Metallic Luste	Powder	F3	Group 1	xxxx	xx	xx		tr	tr	x	x	
	MER6	Relief ware with metallic lustre	Powder	F1	Group 1	xxxx	xx	xx	x	x	tr	x	tr	
	MER7	Relief ware with metallic lustre	Powder	F3	Group 1	xxxx	xx	xx	x	x	tr	x	x	tr
	MER8	Metallic Lustre	Powder	F3	Group 1	xxxx	xx	x	x	tr	tr	x	x	
Coimbra	COI1	Metallic Lustre	Micro	–	Group 1	xxxx	xx	x	x	x	x	x		
	COI2	Metallic Lustre	Micro	–	Group 1	xxxx	xx	x	x	x	x	xx		tr

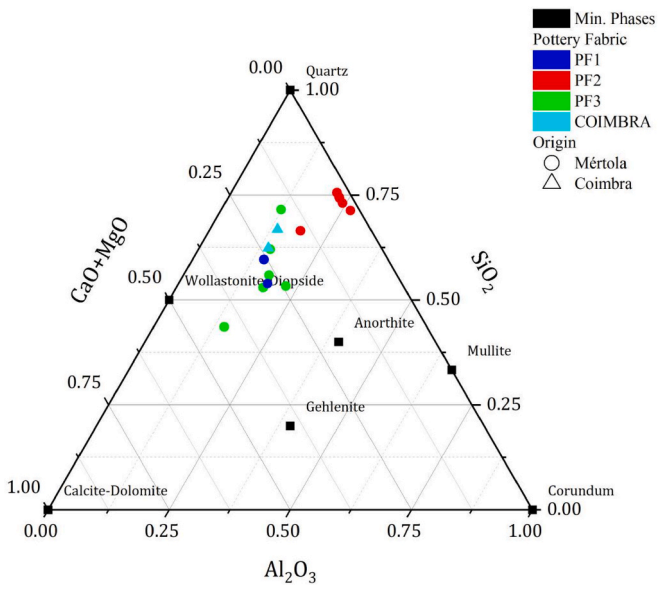

Fig. 5. Samples' ternary plot based on SEM-EDS results.

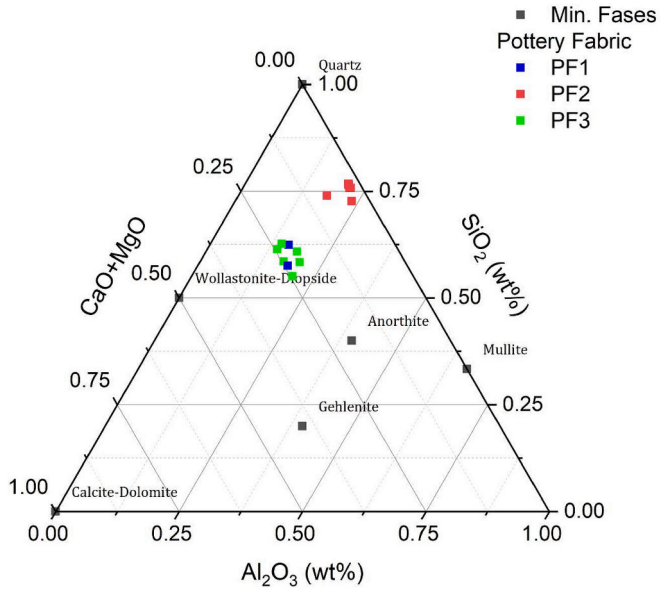

Fig. 6. Samples' ternary plots based on XRF results.

group 2 samples plot within the triangle defined by quartz, anorthite, and mullite (i.e., silica-rich). Considering that gehlenite (identified by XRD) should decompose at high temperature (Heiman & Maggetti, 2019), but it is present in all samples, it is possible to state that samples were not fired at 1100 °C, or the firing time was not sufficient for gehlenite to decompose completely. Nevertheless, sample MER1 (i.e., included in F2–XRD group 1), based on the analysis mode employed, can be plotted within different triangular spaces. XRF results show that it plots inside the silica-rich area (Fig. 6). Conversely, using SEM-EDS data, the sample plots inside the calcium-rich area (Fig. 5). This result indicates that bulk XRF analysis overestimates the SiO_2 concentration within the clay fraction of the ceramic sample MER1, and it confirms that CaO is not included within the temper but rather within the clay matrix. The combination of different optical and analytical methods can be highly fruitful, allowing for a deeper understanding of the chemical contribution of each fraction that makes up the ceramic body. SEM-EDS is clearly more effective for evaluating the thermal history of samples,

especially concerning the transformations involved in the ceramic paste. The difference between the two plots is evident because SiO_2 has a dilution effect, as previously noted in the literature (Beltrame et al., 2021). In our case, these observations underline that sample MER1 perfectly match F2 in terms of temper characteristics as evidenced by OM observations, but the clay fraction is more enriched in CaO. This observation is consistent with the geological variability of the Phyllite/Slate-Quartzite Group (PQ Group)

4.3.2. *Combining SEM-EDS and XRF results: Micro-structure of the ceramic paste.*

The microstructural/chemical analysis of the ceramic paste was developed to determine technological similarities withinfabrics and samples retrieved at *Coimbra*. Samples included in F1 present a fine CaO-rich ceramic paste, poor in temper, and with low oriented porosity. K and Na are generally included inside feldspar grains. F2 samples are characterised by a coarse ceramic paste with abundant non-oriented porosity (Fig. 7A, C). Al, Si and Fe are concentrated in the ceramic paste and quartz crystals, Na, K, and Ca are generally hosted inside feldspars. Ca-rich plagioclases were not observed; most crystals were Na-rich plagioclases. In the case of sample MER1, several high lead glass fragments were also observed. Moreover, in this sample, the chemical distribution of Ca is also different (Fig. 7D), and calcium is also included in the ceramic paste as indicated in the previous section (Section 4.3.1).

Considering fabric F3, the ceramic paste is fine and homogeneous, porosity is much lower and oriented, and temper grain size is smaller when compared to F2. Al and Si are concentrated in the ceramic matrix and in the temper, respectively (Fig. 8B), and Fe is mostly included inside the ceramic paste. K and Na are also generally included inside illite/muscovite phyllosilicates and Na-rich feldspars. Moreover, Na-rich plagioclase grain size decreases significantly if compared to F2 samples. Ca is also included inside the ceramic paste, the carbonate fraction of the employed sediment, and a similar conclusion to sample MER1 can be drawn.

Results obtained from the analysis of samples retrieved at *Coimbra* indicate that the ceramic paste exhibits a significantly different microstructure compared to samples included in F1, 2, and 3. In both cases (samples COI1 and 2), the ceramic body shows extended vitrification and very low/absent porosity (Fig. 9A). The Al and Ca-rich raw material is embedded in a Si-rich amorphous phase (Fig. 9C). Quartz, in addition to K and Na-rich feldspars, was also observed. Moreover, Na and K were also identified in the slip layer applied beneath the glaze (Fig. 9D). The underglaze slip technique has been widely observed on lustreware ceramics from the late Famitid production, in the form of white slip under transparent glaze (Mason, 2004; Pradell et al., 2008a). It is also widely documented in Middle Eastern glazed ceramics, particularly in Iranian examples dated to the 9th–12th centuries (Holakooei et al., 2019). During the 13th century, this practice evolved with the adoption of alkali glazes layered over slips rich in quartz (Molera et al., 2019). The presence of an underglaze slip in the current lustreware samples may suggest an influence from eastern ceramic traditions.

4.3.3. *Combining SEM-EDS and XRF results: Possible provenance*

The results obtained in the previous section revealed specific microstructural characteristics of samples COI1 and COI2, allowing for the identification of distinct technological differences when compared to samples included in F1, F2, and F3. Moreover, ceramic samples retrieved at *Coimbra* show specific chemical characteristics, which corroborate previous observations. These samples exhibit a characteristic depletion in K_2O relative to the other samples (Supplemental file S1), along with a higher concentration of Na_2O. This supports the exploitation of different raw materials, and it is possible to state that COI1 and COI2 samples are not compatible with F1, 2, and 3.

Fabric F1 shows specific differences in bulk chemical composition (i.e. XRF data), with ceramic samples included in fabric F2. Namely, if the binary plot presented in Fig. 10 is considered, it is possible to note sample differences in the Na_2O and K_2O concentrations compared with F2. This difference can be correlated with the feldspars' chemical composition, as well as with specific characteristics of the clay raw material used. So, XRF results support previous observations, indicating

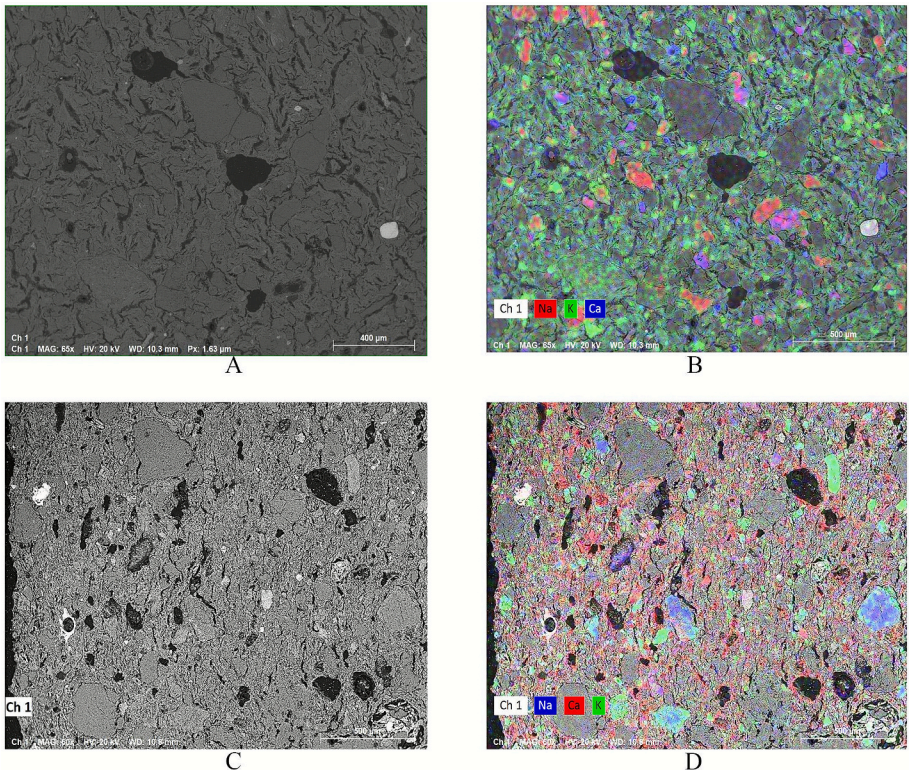

Fig. 7. BSE images (A, C) and elemental mapping distribution of Na, K and Ca (B, D) of samples CW1 (A, B) and MER1 (C, D).

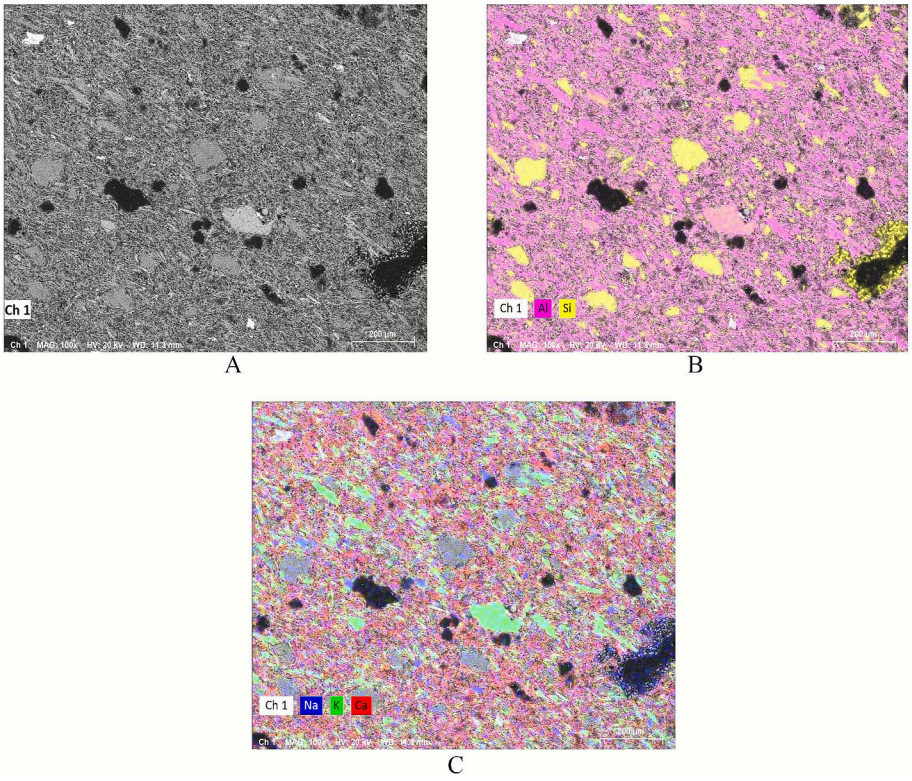

Fig. 8. BSE image (A) and elemental mapping distribution of Al and Si (B) and Na, K and Ca (C) of sample MER4 (PF3).

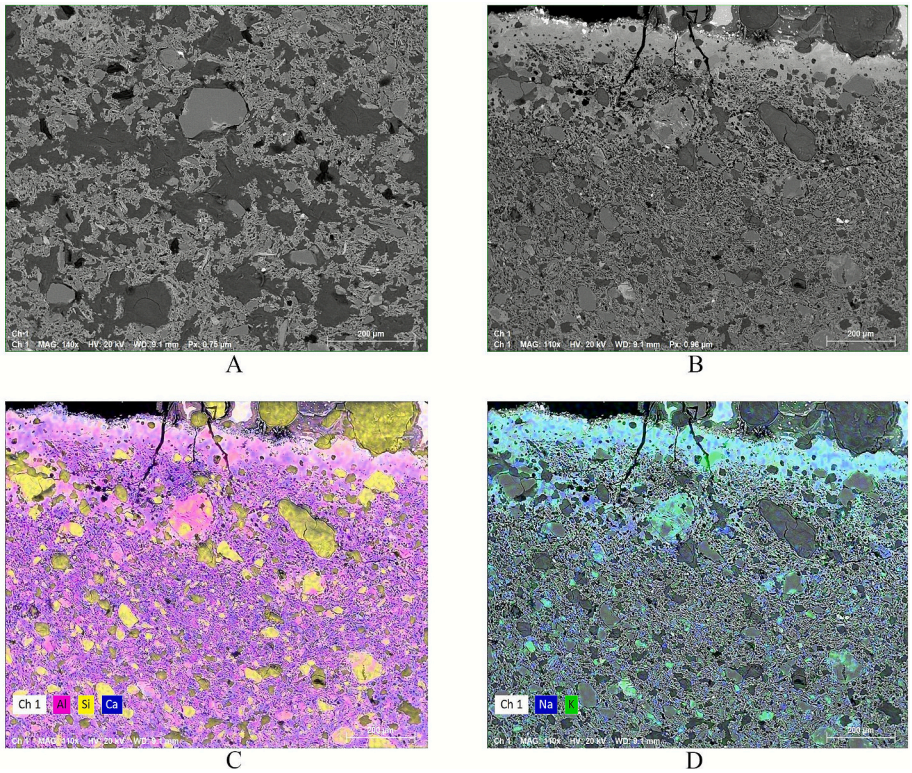

Fig. 9. BSE images and elemental mapping distribution of Al, Si and Ca of samples COI1 (A,C) and COI2 (B,D).

that F1 samples were not produced at *Mértola*.

Regarding the compatibility between F2 and F3, the plot presented in Fig. 10 illustrates how the K_2O concentration varies across different pottery fabrics. K_2O increases inside decorated samples, while Na_2O concentration slightly decreases. This can be attributed to the variation of different mineralogical phases inside the pastes. Micro-analyses results showed that, between F2 and F3, the decrease in temper grain size is associated with an increase in K-rich phyllosilicates, and a decrease in

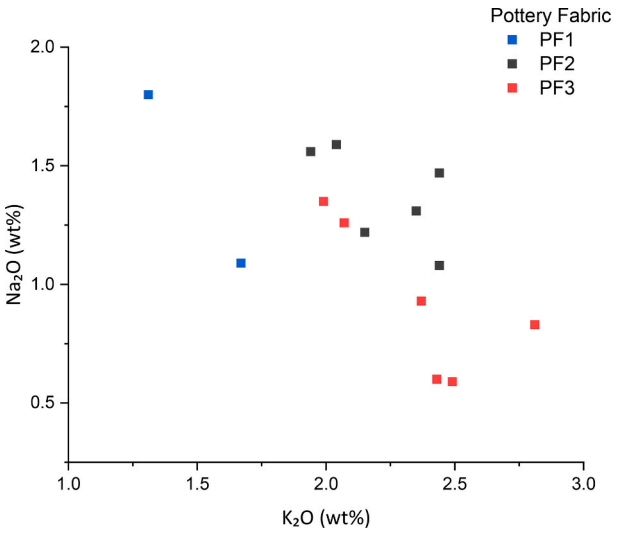

Fig. 10. XRF binary plot presenting the correlation between Na_2O vs K_2O.

Na-rich plagioclase grain size. Therefore, these mineralogical phases are present in different sediment fractions, and they are similar; the presented plot is compatible with the application of different raw material treatments. Moreover, the binary plot presented in Fig. 11B evaluates the distribution of sodium oxide inside Na-rich feldspars, observed in both fabrics. As it can be clearly seen, a linear correlation is shown with Al_2O_3, evidencing that the same feldspar is present in both cases. A similar linear correlation is also observed in the binary plots of Fe_2O_3 vs Al_2O_3 (Fig. 11A), Na_2O vs Fe_2O_3 (Fig. 11D), Al_2O_3 vs Zr (not presented), and Fe_2O_3 vs Rb (not presented). These plots prove striking similarities between the original raw material employed in F2 and F3 at *Mértola*. Basically, the ratio between different major oxides and trace elements is always consistent.

Regarding CaO concentration, the binary plot of CaO vs Al_2O_3 presented in Fig. 11C shows that these two oxides are not linked, and it is the same for most major oxides and trace elements, excluding Sr and MgO. If CaO were included in the original clayey raw material, a linear correlation between these two oxides would be expected, and, for example, the variation in concentration could be influenced by temper addition (i.e. dilution), or different raw material mixing. Conversely, the plot indicates that the carbonate component was originally "isolated" from the clayey fraction of the original employed sediment, supporting, once more, the geological variability of the Phyllite/Slate-Quartzite Group (PQ Group) underlined in section 2. Consequently, the clay and temper fraction of F2 and 3 are the same, the same provenance can be assumed, and the carbonate component has a dilution effect in most major and trace elements.

4.4. SEM-EDS analysis of the Glaze

SEM-EDS analysis was performed on glazed decoration of all the samples, aiming to provide information on the glaze's microstructural/chemical characteristics, glaze type, glaze application technique, firing technique, and the opacification method employed (Pradell & Molera, 2020; Pradell et al., 2013; Tite et al., 1998).

The characteristics of the inner and outer sides of the glaze are shown in Table 5. For the analysis of the chemical composition of the glaze, three areas on the decorated side of each sample were analysed using SEM-EDS. The average values and standard deviations of each oxide, expressed in weight percentage (wt%), were calculated from these measurements and are presented in Table 6 for the outer side and in Table 7 for the inner side.

As presented in Table 7, Sample MER1 exhibits a transparent honey-brown glaze on the outer surface, while the inner surface remains undecorated. Sample MER2 features a black glaze on the exterior and a honey-colored glaze on the interior. Samples MER3, MER7, and MER8 display a white glaze on the outer surface and a honey-colored glaze on the inner surface. MER4, MER5, COI1, and COI2 have white glaze on both surfaces.

Morphologically, the glazes appear mostly homogeneous (Fig. 12B), except those from *Coimbra*, which are more heterogeneous and slightly corroded at the surface. Most samples exhibit vertical cracks and entrapped air bubbles within the glaze layer. The formation of vertical cracks is attributed to minor mismatches in the thermal contraction rates between the ceramic body and the glaze during the cooling process (Tite et al., 1998). The presence of air bubbles (Fig. 12A, C) likely results from the release of gases during the decomposition of organic matter and carbonates (e.g., CO_2, CO), sulphates (SO_2), and the dihydroxylation of clay minerals (OH^-), as well as from residual air or moisture trapped within the glaze (Pradell & Molera, 2020).

Sporadically, unmelted quartz grains can also be found within the glaze (Fig. 12D). This might indicate that the frit employed in glaze

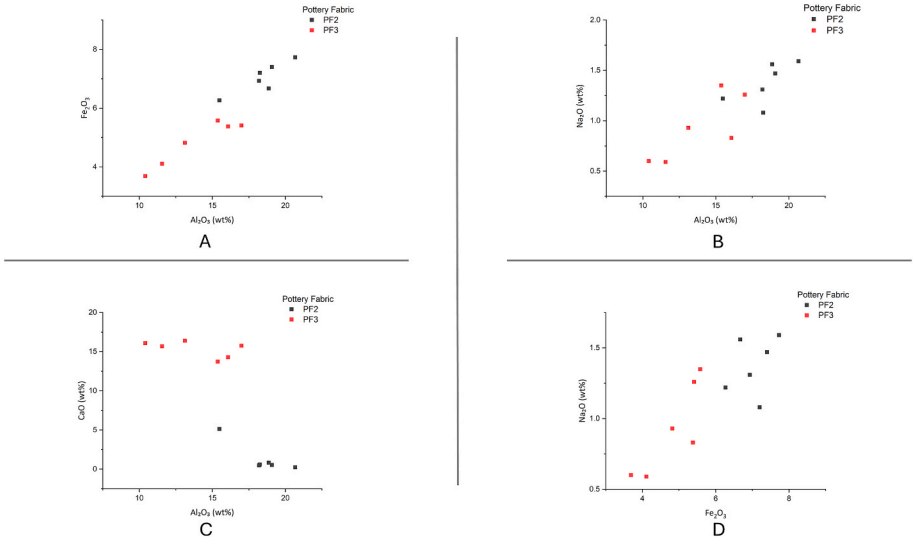

Fig. 11. (A) XRF binary plot representing the correlation of Fe_2O_3 and Al_2O_3 of the samples from PF2 and PF. (B) XRF binary plot representing the correlation of Na_2O and Al_2O_3 of the samples from PF2 and PF3. (C) XRF binary plot representing the correlation of CaO and Al_2O_3 of the samples from PF2 and PF3. (D) XRF binary plot representing the correlation of Na_2O and Fe_2O_3 of the samples from PF2 and PF3.

Table 5
Characteristics of the inner and outer sides of the glaze of all samples observed with SEM-EDS.

Sample	Typology	Inner/ outer glaze	Glaze thickness (μm)	Colour	Alteration	Crack	Air bubbles	Glaze application technique	Firing technique	Interface thickness, μm	Glaze type	Homogenity	Opacificant	SnO_2 morphology	Quartz grains
MER1	Jar	inner	–	–	–	–	–	–	–	–	–	–	–	–	–
		outer	108–166	Honey-Brown	No	No	No	Frit	Double firing	19–26	High-lead	Yes	No	–	Yes
MER2	Jar	Inner	307–352	Honey	Corrosion	Yes	Yes	Frit	Double firing	48–86	High-lead	No	No	–	No
		Outer	302–400	Black	Corrosion	Yes	Yes	Frit	Double firing	40–53	High-lead	No	No	–	No
MER3	Jar	Inner	183–126	Honey	Corrosion	Yes	Yes	Frit	Double firing	26.2–32	High-lead alkali	No	No	–	Yes
		Outer	264–276	White	Corrosion	Yes	Yes	Frit	Double firing	16	High-lead alkali	No	Yes	Granular and acircular grains dispersed in the glaze	Yes
MER4	Bowl	Inner	189	White	Corrosion	Yes	Yes	Frit	Double firing	15	High-lead alkali	Yes	Yes	Granular and acircular grains dispersed in the glaze	Yes, some
		Outer	130–140	White	Corrosion	Yes	Yes	Frit	Double firing	5–20	High-lead alkali	Yes	Yes	Granular and acircular grains dispersed in the glaze	Yes, some
MER5	Bowl	Inner	390	White	Corrosion	Yes	Yes	Frit	Double firing	12–25	High-lead alkali	Yes	Yes	Granular and acircular grains dispersed in the glaze	Yes
		Outer	180–190	White	Corrosion	Yes	Yes	Frit	Double firing	5–20	High-lead alkali	Yes	Yes	Granular and acircular grains dispersed in the glaze	Yes
MER6	Jar	Inner	220–258	White	Corrosion	Yes	Yes	Frit	Double firing	33.2–43.6	High-lead alkali	Yes	No	–	No
		Outer	148–196	White	Corrosion	Yes	Yes	Frit	Double firing	19.4–31.3	High-lead alkali	Yes	Yes	Granular and acircular grains dispersed in the glaze	No
MER7	Jar	Inner	56,2–58	Honey	Corrosion	Yes	Yes	Frit	Double firing	12–17	High-lead alkali	Yes	No	–	No
		Outer	128–140	Green	Corrosion	Yes	Yes	Frit	Double firing	8–15	High-lead alkali	Yes	Yes	Granular and acircular grains dispersed in the glaze	Yes
MER8	Jar	Inner	50–60	Honey	Corrosion	Yes	Yes	Frit	Double firing	20–40	High-lead alkali	Yes	No	–	No
		Outer	155–175	White	Corrosion	Yes	Yes	Frit	Double firing	8–15	High-lead alkali	Yes	Yes	Granular and acircular grains dispersed in the glaze	No
COI1	Bowl	Inner	147–153	White	Corrosion	Yes	Yes	Frit	Double firing	40–74	Alkali-lead	No	Yes	Granular and acircular grains dispersed in the glaze	Yes
		Outer	155–165	White	Corrosion	Yes	Yes	Frit	Double firing	39–68	Alkali-lead	No	Yes	Granular and acircular grains dispersed in the glaze	Yes
COI2	Bowl	Inner	360–370	White	Corrosion	Yes	Yes	Frit	Double firing	Not visible	Alkali-lead	No	Yes	Granular and acircular grains dispersed in the glaze	Yes
		Outer	420–440	White	Corrosion	Yes	Yes	Frit	Double firing	Not visible	Alkali-lead	No	Yes	Granular and acircular grains dispersed in the glaze	Yes

Table 6
Medium Values (AVR) in oxides wt% with Standard Deviation (SD) from the outer side of the samples.

SAMPLE	ORIGIN	SIDE	F	Na_2O	MgO	Al_2O_3	SiO_2	PbO	P_2O_5	TiO_2	Fe_2O3	CaO	K_2O	CuO	MnO	SnO_2	Cl
MER1 AVR	MERTOLA	OUTSIDE	2	1.07	0.64	6.54	41.97	35.76	0	0.33	4.2	6.42	3.02	0	0	0	0
SD				0.05	0.13	0.39	1.63	1.4	0	0.23	0.07	0.3	0.1	0	0	0	0
MER2 AVR	MERTOLA	OUTSIDE	3	0.89	0.53	3.91	32.71	53.45	0	0.23	1.58	3.67	1.48	0	1.25	0	0.3
SD				0.03	0.11	0.73	0.16	1	0	0.03	0.09	0.18	0.2	0	0.16	0	0.19
MER3 AVR	MERTOLA	OUTSIDE	3	3.26	0.46	0.76	39.51	44.23	0	0.02	0.66	2.89	1.87	0	0	6.32	0
SD				0.08	0.12	0.11	0.8	1.21	0	0.02	0.14	0.14	0.08	0	0	0.54	0
MER4 AVR	MERTOLA	OUTSIDE	3	4.96	1.08	1.06	41.16	39.86	0	0.05	0.72	4.25	2.66	0	0	4.2	0
SD				0.03	0.08	0.19	0.71	0.32	0	0.04	0.15	0.38	0.04	0	0	0.28	0
MER5 AVR	MERTOLA	OUTSIDE	3	3.09	0.73	2.79	40.88	39.95	0.00	0.14	1.86	4.52	2.52	0.00	0.00	3.53	0
SD				0.19	0.12	0.1	0.65	1.4	0	0.03	0.03	1.18	0.11	0	0	1.67	0
MER6 AVR	MERTOLA	OUTSIDE	1	2.31	1.01	1.87	33.71	44.41	0	0.21	0.98	5.12	2.53	0.02	0	7.87	0
SD				0.06	0.04	0.57	0.36	0.4	0	0.15	0.17	0.33	0.16	0.02	0	1.15	0
MER7 AVR	MERTOLA	OUTSIDE	3	4.12	1.84	2.18	47.88	28.49	0.74	0.05	1.07	5.48	4.48	0.42	0	3.37	0
SD				0.14	0.07	0.75	0.26	1.99	0.39	0.01	0.27	0.87	0.18	0.08	0	0.27	0
MER8 AVR	MERTOLA	OUTSIDE	3	4.63	1.78	2.53	46.75	30.65	0	0.07	1.15	5.53	4.55	0	0	2.36	0
SD				0.25	0.06	0.6	0.76	0.84	0	0.03	0.02	0.27	0.23	0	0	0.23	0
COI1 AVR	*COIMBRA*	OUTSIDE	–	6.87	3.77	2.87	59.66	6.72	0.18	0.12	1.5	7.78	5.36	0.04	0.31	4.83	0
SD			–	0.11	0.15	0.08	1.03	0.26	0.04	0.04	0.06	0.14	0.11	0.02	0.01	1.11	0
COI2 AVR	COIMBR	OUTSIDE	–	5.73	3	2.87	58.9	10.52	0.2	0.07	1.42	4.23	5.33	0.44	0.06	7.24	0
SD			–	0.65	0.22	1.35	1.49	1.04	0.03	0.04	0.05	0.42	0.2	0.51	0.03	1.73	0

preparation was not accurately milled and sieved in all cases before application (Tite et al., 1998; Walton & Tite, 2010; Pradell & Molera,2020). Opacification is always obtained using SnO_2 particles dispersed in the glass in the form of acicular or slightly granular crystallites, being relatively abundant on *Coimbra* samples (Fig. 12A).

The morphological information observed in the glaze by BSE images also provides insight into the ceramics' firing technology. Glaze can be applied on top of raw (single firing) or already fired ceramic bodies (double firing) (Tite et al., 1998; Molera et al., 2001; Pradell & Molera, 2020). The method used can be determined by examining the interaction layer between the glaze and the ceramic paste (the interface). More specifically, when the glaze is applied to unfired ceramics, there is greater interaction between the ceramic support and the glaze, resulting in a thicker interface and a greater digestion of the ceramic body (Molera et al., 2001; Tite et al., 1998). The samples examined exhibit a limited development of the glaze/ceramic paste interface, ranging from 5 to 86 μm, which indicates that the glaze was applied to biscuit-fired clay bodies.

Two distinct chemical groups of glaze types have been identified: high-lead alkali and alkali-lead. Ceramic samples from *Coimbra* correspond to the alkali-lead glaze type, whereas the glaze applied to the *Mértola* samples is characterised as the high lead–alkali type (Pradell & Molera, 2020). The alkali-lead glaze type found in the two *Coimbra* samples (Tite et al., 1998) is not traditionally used in the Iberian Peninsula but was mainly employed in Iraqi (Pradell & Molera, 2020) and Egyptian (Garofano et al., 2015; Pradell & Molera, 2020) workshops. This is consistent with the underglaze slip observed in Section 4.3.2, which is also considered a traditional Eastern practice (Holakooei et al., 2019; Molera et al., 2019; Taxel, 2014; Whitcomb, 1989; Mason, 2004; Pradell et al., 2008a; Scanlon, 1998). The glaze technology and the presence of an underglaze slip in the current samples may therefore suggest a connection with Fatimid tradition.

The Na_2O vs. SiO_2 plots for both the outer (Fig. 13A) and the inner (Fig. 13B) glaze surfaces highlight the technological differences between the samples. In both graphs, the decorated samples from F1 and F3 exhibit a linear correlation between Na_2O and SiO_2, whereas the *Coimbra* samples, which also have a linear correlation, stand out with notably higher concentrations of both Na_2O and SiO_2, reflecting a distinct production tradition. Sample MER2 (F2) appears only in the plot for the outer surface, as only this surface is decorated. It does not cluster with the other *Mértola* samples due to its deficiency in Na_2O, despite having a similar SiO_2 content to F3.

The technological correlation between the samples retrieved at *Mértola* and the correlation between the two *Coimbra* samples is even more evident in the plots of SiO_2/PbO vs. $Na_2O + K_2O$ (Fig. 13C and D). Although the $Na_2O + K_2O$ percentage fluctuates significantly lower for the *Mértola* samples, the SiO_{22}/PbO ratio is almost identical for all samples recovered at *Mértola*. Regarding glaze colourants, the honey colour of the glaze observed on the inner surface of various samples and the honey-brown colour on the outer surface of sample MER1 is attributed to the presence of Fe_2O_3 (Molera et al., 2018; Tite et al., 2015; Salinas et al., 2018). Additionally, the black glaze on the outer surface of sample MER2 is attributed to the presence of MnO (Molera et al., 2013; Camara et al., 2023). Finally, the green glaze on the outer surface of sample MER7 is attributed to the presence of CuO (Molera et al., 2018; Pradell & Molera, 2020; Salinas et al., 2018). In all cases, the colourants are dissolved in the glaze.

The white glaze on the lustreware and relief-lustreware samples is opacified by the presence of SnO_2, with concentrations ranging from 2 % to 14 %. The *Coimbra* samples exhibit higher SnO_2 content compared to the *Mértola* samples, and a large number of Sn particles are visibly dispersed within the glaze matrix (Fig. 12A). As previously noted, tin was widely employed as an opacifier in glaze technology, first appearing in Egypt and subsequently in Syria during the late 7th to 8th centuries AD. Its use later became prominent in the production of opaque white glazes in Abbasid Iraq in the 9th century CE (Watson, 2014; Tite et al., 2015).

The production of tin-opacified, lead-alkali glazes involves creating a suspension composed of a lead compound, silica, tin oxide, and an alkali. Initially, a mixture of lead and tin is calcined, heated in the presence of oxygen, to produce a powdered oxide known as *calx* (Matin et al., 2018). To achieve the characteristic opaque white glaze, the *calx* is combined with silica and an alkaline frit, prepared by first fusing the water-soluble alkali with silica to form a stable compound, and then subjected to further heating (Tite et al., 1998). In accordance with this method, all tin-opacified, lead-alkali glaze samples produced in this study were prepared using a fritted mixture. As an alkaline source, the elevated Na_2O content in the glaze of the tin-opacified samples, compared to that of the ceramic paste, may indicate the use of plant ashes. This is consistent with Abbasid recipes for tin-glazed wares and has also been observed in an assemblage of polychrome tin-glazed ceramics from *Córdoba* (Salinas & Pradell, 2020b). Consequently, even with differences in ceramic provenance, a homogenous glaze technology has been observed at *Mértola*, indicating technological transfer amongst different places.

Table 7
Medium Values (AVR) in oxides wt% with Standard Deviation (SD) from the inner side of the samples.

SAMPLE	ORIGIN	SIDE	F	Na_2O	MgO	Al_2O_3	SiO_2	PbO	P_2O_5	TiO_2	Fe_2O_3	CaO	K_2O	Cl	CuO	SnO_2
MER1 AVR	MERTOLA	OUTSIDE	2	Undecorated	Undecorated	Undecorated	Undecorated	Undecorated	Undecorated	Undecorated	Undecorated	Undecorated	Undecorated	Undecorated	Undecorated	Undecorated
SD				–	–	–	–	–	–	–	–	–	–	–	–	–
MER2 AVR	MERTOLA	INSIDE	2	0.30	0.37	2.27	32.54	58.90	0.00	0.11	1.22	3.59	0.43	0.00	0.00	0.00
SD			2	0.03	0.01	0.45	0.06	1.09	0.00	0.04	0.09	0.55	0.08	0.03	0.00	0.00
MER3 AVR	MERTOLA	INSIDE	3	0.68	0.50	3.80	35.29	50.65	0.53	0.23	1.93	5.18	1.21	0.00	0.00	0
SD			3	0.12	0.10	1.00	0.59	2.46	0.23	0.06	0.36	0.31	0.15	0.00	0.00	0.12
MER4 AVR	MERTOLA	INSIDE	3	3.78	1.24	1.44	40	40.61	0.53	0	0.65	4.53	3.02	0.00	0.00	4.24
SD			3	0.20	0.04	0.14	1.25	1.28	0.69	0.00	0.08	0.43	0.09	0.00	0.00	0.20
MER5 AVR	MERTOLA	INSIDE	3	2.36	1.01	2.11	36.49	39.71	0.00	0.08	0.89	3.62	4.39	0.00	0.00	9.34
SD			3	0.02	0.09	0.39	1.18	0.91	0.00	0.02	0.23	0.39	0.11	0.00	0.00	2.43
MER6 AVR	MERTOLA	INSIDE	1	1.10	0.81	3.06	34.37	51.73	0.00	0.23	1.29	5.45	1.97	0.00	0.00	0.00
SD			1	0.05	0.03	0.29	0.60	1.20	0.00	0.01	0.12	0.19	0.07	0.00	0.00	0.00
MER7 AVR	MERTOLA	INSIDE	3	0.86	0.68	5.80	28.73	52.18	0.19	0.39	2.80	6.13	2.25	0.00	0.00	0.00
SD			3	0.04	0.05	0.24	0.40	0.81	0.05	0.04	0.09	0.22	0.07	0.00	0.00	0.00
MER8 AVR	MERTOLA	INSIDE	3	3.11	0.75	7.23	42.59	31.85	0.00	0.48	4.36	3.71	5.92	0.00	0.00	0.00
SD			3	0.13	0.09	0.17	0.75	0.63	0.00	0.06	0.19	0.22	0.12	0.00	0.00	0.00
COI1 AVR	*COIMBRA*	INSIDE	3	6.17	3.58	2.60	59.87	5.31	0.16	0.13	1.48	7.36	5.50	0.47	0.02	7.36
SD			3	0.27	0.22	0.08	1.23	0.19	0.01	0.03	0.16	0.08	0.06	0.03	0.03	0.71
COI2 AVR	*COIMBRA*	INSIDE	–	6.18	2.88	1.97	56.80	10.89	0.00	0.09	1.24	3.81	5.02	0.00	0.54	10.58
SD			–	0.32	0.05	0.11	2.13	0.87	0.00	0.02	0.08	0.30	0.11	0.00	0.02	2.42

4.5. *FEG-SEM TESCAN CLARA analysis of the lustre*

SEM-EDS analysis was successfully performed in five samples, while the observation of the lustre was unsuccessful in the rest. The results of the observations are briefly shown in Table 8. The lustre nanoparticles of sample COI2 and the lustre layer of sample MER8 are shown in Fig. 14 and Fig. 15, respectively.

The lustre colours on the surface of the samples varied, with the *Coimbra* samples having a brown and amber colour, and samples from Mértola, MER7, and MER8 both presented a red colour; sample MER3 exhibited a golden-brown colour.

The *Mértola* samples exhibited a metallic shine, attributed to Pb's presence in the glaze (Pradell, Molera, et al., 2008). Samples from *Coimbra* do not exhibit a metallic shine, which is related to the chemical composition of the glaze, which only contains 1–6 % PbO.

As mentioned in Section 1, the production of the lustre layer involves a complex process driven by an ionic exchange between alkali ions from the glaze and silver and copper ions in the applied paint (Pradell & Molera, 2020), which makes alkalis a necessity. This is why alkalis were present in the glaze of all the lustreware and relief-lustreware samples.

Regarding the lustre composition, as observed in Table 3, the two *Coimbra* samples contain Cu and Ag nanoparticles, which are compatible with brown and amber lustre colours. The samples MER7 and MER8 found in *Mértola* only contain Cu, which again justifies the red colour (Pradell et al., 2008). Regarding sample MER3, the concentration of both Ag and Cu is compatible with the golden-brown colour of the lustre.

By comparing the layer thickness between the samples, we can observe that MER3, MER7 and MER8 have a significantly narrower lustre layer (0.07–0.1 for sample MER3, 0.17–0.22 μm for sample MER7 and 0.12–0.16 μm for samples MER8) than the *Coimbra* samples (5.64–10.98 μm for sample COI2 and 5.6–7.9 μm for sample COI1) This fact is again related to the presence of Pb in the glaze, as lead decreases ionic mobility, resulting in the accumulation of metal nanoparticles closer to the surface. (Pradell & Molera, 2020).

Considering the lustre technology, the samples from *Coimbra* exhibit copper/silver brown and amber colours and lack metallic shine. The simultaneous use of copper and silver nanoparticles is another resemblance with a sample found at *Seville* that originates from Egypt or Iraq (Garofano et al., 2015). Additionally, the lustre technology that migrated to the West utilises lead-rich and tin-opacified glazes on calcareous pastes (Pradell et al., 2008), similar to the technology employed in the lustreware samples from *Mértola.* Therefore, this agrees with the conclusion that these samples were produced in the Iberian Peninsula.

Regarding the firing process, the ionic exchange between alkali ions from the glaze and silver and copper ions in the requires firing at relatively low temperatures, typically between 500 °C and 600 °C (Pradell et al., 2008b). Regarding the firing conditions, the two samples from *Coimbra*, containing both Cu and Ag, were fired under high-reducing conditions, as amber colour requires these kinds of conditions. In contrast, golden brown from the *Mértola* sample was obtained under much less reducing conditions (Pradell et al., 2008a, 2008b).

5. Conclusions

Provenance of the Lustreware Samples from *Mértola*

The integration of mineralogical, petrographic, micro-structural, and compositional data supports the local production of the relief, lustre and relief-lustrewares recovered at *Mértola*. Fabric 2 (F2) was identified as a local ceramic production based on the compatibility of its common wares—both morphologically and mineralogically—with two kiln samples excavated in situ. Furthermore, the inclusions within the ceramic paste correlate well with the regional geological context, strengthening the attribution to a local origin.

Comparative analysis using Optical Microscopy revealed strong mineralogical and textural similarities between the common ware

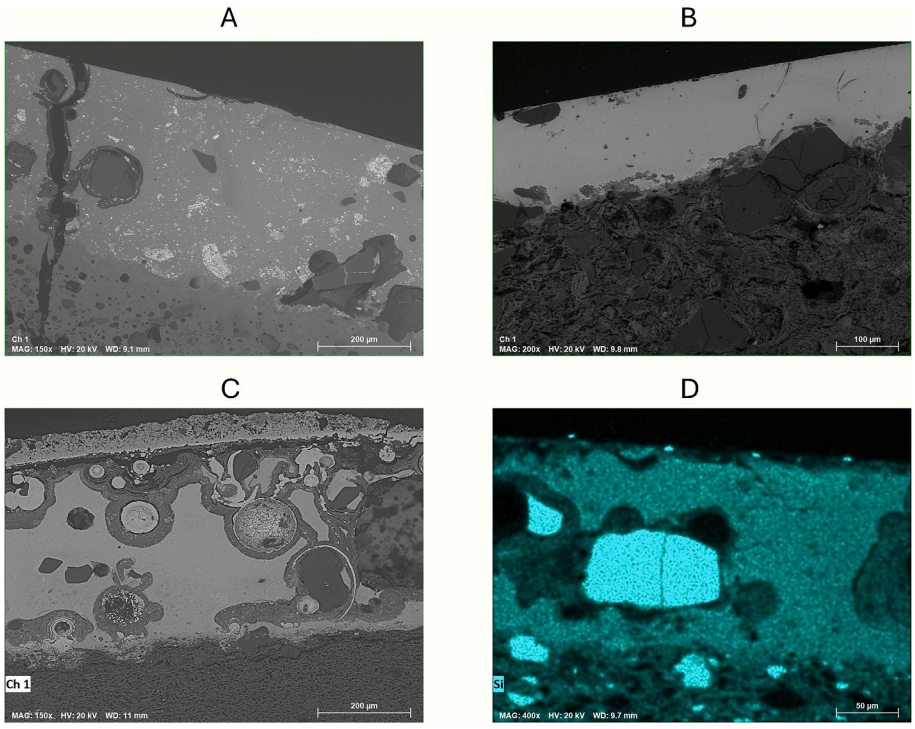

Fig. 12. (A) BSE image of the outer surface of the lusterware sample from Coimbra (COI2) presenting corrosion and tin particles in the glaze. (B) BSE image of the decorated surface of sample MER1 from Mértola. The glaze appears to be very homogeneous, with one quartz grain visible at the top right. (C) BSE image of the inner surface of the MER sample from Mértola. The glaze contains quartz grains and is also highly corroded. (D) Inner surface of sample MER7. A large grain of quartz is observed.

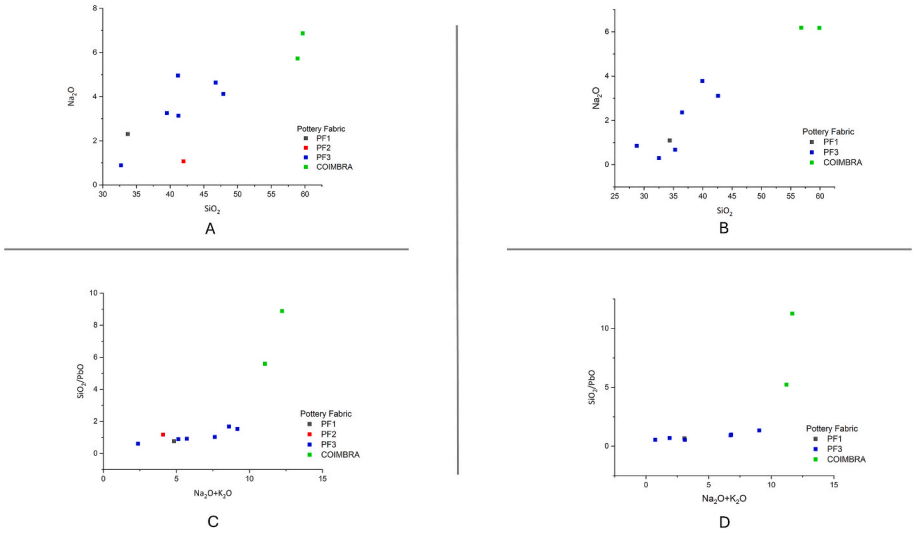

Fig. 13. (A) Na_2O vs. SiO_2 plot of the outer side of the samples. (B) Na_2O vs. SiO_2 plot of the inner side of the samples (C) SiO_2/PbO vs $Na_2O + K_2O$ plot of the inner side of the samples (D) SiO_2/PbO vs $Na_2O + K_2O$ plot of the outer side of the samples.

Table 8
Results of SEM analysis of the lustre and relief-lustre samples.

Sample	Origin	Lustre Colours	Lustre Condition	Metallic Shine	Composition wt% Cu	Composition wt% Ag	Particle Size (nm)	Layer Thickness (µm)
COI1	*Coimbra*	Brown and amber	Preserved	No	4.73	2.03	21.34–45.96	5.6–7.09
COI2	*Coimbra*	Brown and amber	Preserved	No	4.01	1.47	14.94–86.33	5.92–10.98
MER3	*Mértola*	Golden/Brown	Preserved	Yes	2.95	5.70	20.2–26.6	0.07–0.1
MER4	*Mértola*	Not preserved	Partially preserved	Not preserved	No	No	No data	No data
MER5	*Mértola*	Not preserved	Partially preserved	Not preserved	No	No	No data	No data
MER6	*Mértola*	Not preserved	Partially preserved	Not preserved	No	No	No data	No data
MER7	*Mértola*	Red	Preserved	Yes	8.85	0	32–53.5	0.18–0.22
MER8	*Mértola*	Red	Preserved	Yes	2.92	0	17.7–71.4	0.12–0.16

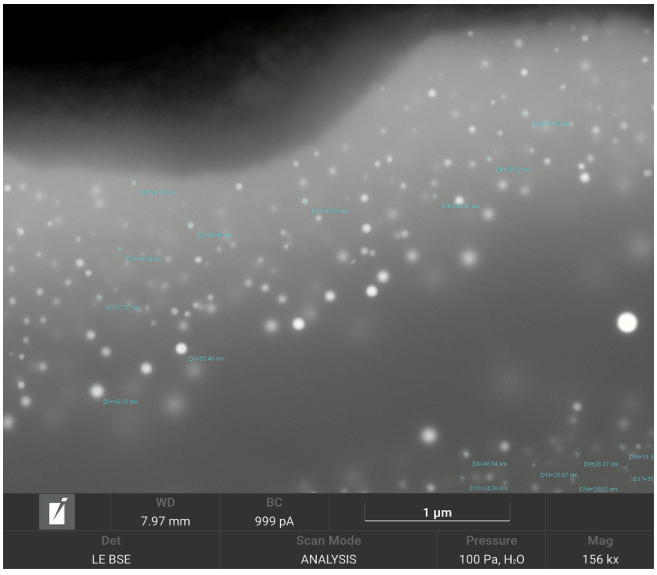

Fig. 14. Particle measurements from the lustre layer of sample COI2.

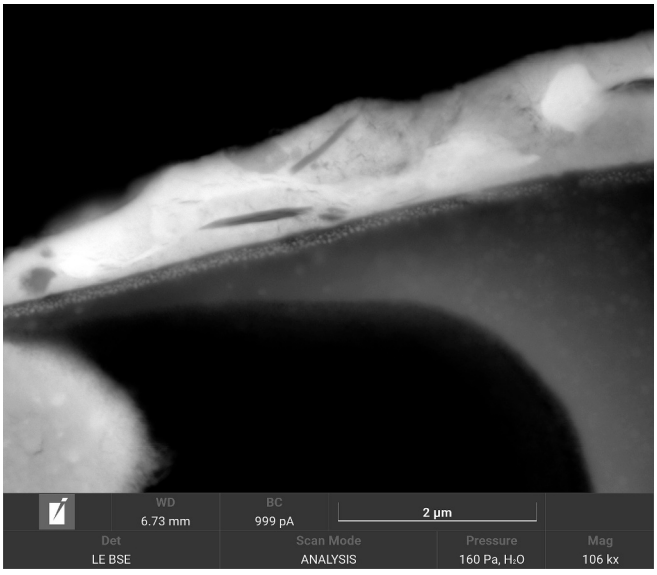

Fig. 15. BSE image of the lustre layer of the sample MER8.

samples (F2) and the relief, lustre and relief-lustre assemblage (F3), except for sample MER6 and sample CW4. These groups share similar inclusions and paste characteristics, indicating that the same or similar raw materials were employed in both productions. However, differences in temper grain size suggest deliberate modifications to the raw material for lustreware production, likely to enhance its suitability for glazing.

Although XRD analysis categorised the *Mértola* ceramics into calcareous (decorated) and non-calcareous (common ware) clays, further geochemical data from XRF showed consistent linear correlations between different major oxides and trace elements, indicating the use of geochemically compatible clay sources. The principal difference appears to lie in the calcium content, and it is attributed to the geological variability of the Phyllite/Slate-Quartzite Group (PQ Group). These findings support the conclusion that the *Mértola* relief, lustre and relief-lustre assemblage was produced locally, contributing a previously undocumented production centre to the broader network of lustreware workshops in the Iberian Peninsula. Samples recovered at Coimbra are linked to the Middle East ceramic technology tradition, indicating they were imported into the Iberian Peninsula.

Glaze production technology

Elemental analysis of the glaze layers distinguishes two primary technological traditions. Samples from *Mértola* (excluding MER1 and MER2) are characterised by white, tin-opacified, high-lead alkali glazes, while those from *Coimbra* correspond to a tin-opacified, low-lead alkali glaze, on top of a slip a type predominantly associated with eastern Islamic production.

The variation in glaze colours observed across the samples is attributed to the presence of specific colourants. The honey-colored glaze visible on the inner surfaces of several samples and the honey-brown glaze on the outer surface of sample MER1 is due to the presence of Fe_2O_3. The black glaze found on the outer surface of sample MER2 results from the presence of MnO. Finally, the green glaze observed on the outer surface of sample MER7 is linked to the presence of CuO.

In addition to the technological distinction revealed by elemental analysis of the glaze, the binary plots of $Na_2O + K_2O$ and SiO_2/PbO vs $Na_2O + K_2O$ revealed two compositional clusters corresponding to the geographic origin of the samples, consistent with the ceramic body analyses.

Lustre production technology

SEM-EDS analysis of the lustre layers revealed three distinct technological approaches across the studied assemblage. The *Coimbra* samples exhibit copper and silver nanoparticles but lack the characteristic metallic sheen, aligning them with lustreware produced in Iraq and Fatimid Egypt. This supports the hypothesis that these fragments represent imported eastern wares.

In contrast, the *Mértola* samples show variable compositions: MER7 and MER8 contain only copper, while MER3 contains both silver and copper. These compositions correspond to red (Cu) and golden-brown (Cu + Ag) lustre colours, respectively.

The presence of thin lustre layers in the *Mértola* samples, associated with lead-rich glazes, is characteristic of Iberian lustre technology, where lead reduces ionic mobility and concentrates metallic nanoparticles near the surface. These technological features, lead- and tin-rich glazes applied to calcareous bodies, are consistent with known production strategies within the Iberian Peninsula.

Together, these data demonstrate that while some lustreware was imported (e.g., the *Coimbra* samples), *Mértola* was an active centre of lustreware and lustre-relief ware production, employing distinct yet locally adapted technological traditions.

CRediT authorship contribution statement

Stamatina Nikologianni: Writing – review & editing, Writing – original draft, Visualization, Validation, Software, Methodology, Investigation, Formal analysis, Data curation, Conceptualization. **José Mirao:** Writing – review & editing. **Susana Gómez Martínez:** Writing – review & editing. **Nicola Schiavon:** Writing – review & editing. **Luis Dias:** Writing – review & editing. **Helena Catarino:** Writing – review & editing. **Elena Salinas:** Writing – review & editing. **Massimo Beltrame:** Writing – review & editing, Writing – original draft, Visualization, Validation, Supervision, Project administration, Funding acquisition, Data curation, Conceptualization.

Declaration of competing interest

The authors declare that they have no known competing financial interests or personal relationships that could have appeared to influence the work reported in this paper.

Acknowledgements

This manuscript has been developed in the framework of the exploratory project “GC-CIGA Glaze Ceramic Introduction and

Consumption in the Gharb al-Andalus, granted by the Portuguese FCT to the corresponding author. Project code: 2023.13937.PEX, DOI: DOI: 10.54499/2023.13937.PEX. The research team wish to acknowledge the FCT for funding the Hercules Laboratory (UIDB/04449/2025).

Appendix A. Supplementary material

Supplementary data to this article can be found online at https://doi.org/10.1016/j.jasrep.2025.105494.

Data availability

Data will be made available on request.

References

Almodóvar, G.R., Yesares, L., Sáez, R., Toscano, M., González, F., Pons, J.M., 2019. Massive sulfide ores in the Iberian Pyrite Belt: mineralogical and textural evolution. Minerals 9 (11), 653. https://doi.org/10.3390/min9110653.

Barceló, C., Heidenreich, A., 2014. Lusterware made in the Abbadid Taifa of Seville (Eleventh century) and its early production in the Mediterranean region. Muqarnas Online 31 (1), 245–276. https://doi.org/10.1163/22118993-00311p10.

Beltrame, M., Liberato, M., Mirão, J., Santos, H., Barrulas, P., Branco, F., Gonçalves, L., Candeias, A., Schiavon, N., 2019. Islamic and post-Islamic ceramics from the town of Santarém (Portugal): the continuity of ceramic technology in a transforming society. J. Archaeol. Sci. Rep. 23, 910–928. https://doi.org/10.1016/j.jasrep.2018.11.029.

Beltrame, M., Sitzia, F., Arruda, A.M., Barrulas, P., Barata, F.T., Mirão, J., 2021. The islamic ceramic of the santarém alcaçova: raw materials, technology, and trade. Archaeometry 63 (6), 1157–1177. https://doi.org/10.1111/arcm.12671.

Beltrame, M., Branco, C., Mirao, J., Gonçalves, L.J., 2022. CALIPH: Comprehensive Archaeological and laboratory investigation of Islamic pottery in Portuguese History. [Doctoral Dissertation, Universidade de Évora, Repositorio Universidade de Évora. https://dspace.uevora.pt/rdpc/handle/10174/31377.

Caiger-Smith, A., 1991. Lustre Pottery. Herbert Press.

Camara, C.A., Gonçalves, M.J., Mirão, J.A.P., Martínez, S.G., Beltrame, M., 2023. High-Lead glazed ceramic production in Western Iberia (*Gharb al-Andalus*) between the 10th and Mid-13th Centuries: an approach from the city of Évora (Portugal). Ceramics 6 (4), 2213–2242. https://doi.org/10.3390/ceramics6040135.

Camara, C.A., Lopes, G., Schiavon, N., Mirão, J., Beltrame, M., 2025. Islamic Middle Ages Pottery from Muge (Portugal), Serradinho Archaeological Site—A Long-Lasting tradition of Pottery Production. Ceramics 8 (2), 31. https://doi.org/10.3390/ceramics8020031.

Carboni, S., 2001. *Glass from Islamic lands*. Thames & Hudson.

Catarino, H., Filipe, S., Santos, C.D., 2009. Coimbra islâmica: uma aproximação aos materiais cerâmicos. XELB 9 - 6° Encontro de Arqueologia do Algarve, 2009, pp. 333–378.

Duda, D., 1970. Spanisch-islamiche keramik aus Almería. Von 12 bis 15 Jahrhundert. Heidelberg.

Fabbri, B., Gualtieri, S., Shoval, S., 2014. The presence of calcite in archeological ceramics. J. Eur. Ceram. Soc. 34 (7), 1899–1911. https://doi.org/10.1016/j.jeurceramsoc.2014.01.007.

Fernández Gabaldón, S., 1987. El yacimiento de la Encarnación (Jerez de la Frontera): bases para la sistematización tipológica de la cerámica almohade en el S.O. Peninsular. Al-Qantara. Madrid-Granada: CSIC. ISSN 0211-3589. Vol. VIII, pp. 448-474.

Ferreira, L.F.V., Gomes, R.V., Pereira, M.F.C., Santos, L.F., Machado, I.F., 2016. Islamic ceramics in Portugal found at Silves Castle (8th to 13th c.): an archaeometric characterization. J. Archaeol. Sci. Rep. 8, 434–443. https://doi.org/10.1016/j.jasrep.2016.06.051.

Flores Escobosa, I., Navarro Ortega, A.D, 2012. Moldes y cerámica moldada y dorada fabricada en Almería. In Patronato de la Alhambra y Generalife (Ed.), Actas del I Congreso Red Europea de Museos de Arte Islámico (REMAI) (pp. 253–270). Patronato de la Alhambra y Generalife.

Garofano, I., Robador, M., Perez-Rodriguez, J., Castaing, J., Pacheco, C., Duran, A., 2015. Ceramics from the Alcazar Palace in Seville (Spain) dated between the 11th and 15th centuries: compositions, technological features and degradation processes. J. Eur. Ceram. Soc. 35 (15), 4307–4319. https://doi.org/10.1016/j.jeurceramsoc.2015.07.033.

Varela Gomes, R.. 1991. Cerâmicas Almóadas do Castelo De Silves. In A Cerâmica Medieval no Mediterrâneo. Lisboa, 1987. Mértola: Campo Arqueológico de Mértola. P. 387-403.

Gómez-Martínez, S., 1997. Loiça dourada de Mértola. Arqueologia Medieval, 5, 137–162.

Gómez-Martínez, S., 2003. Producciones cerámicas en la Mértola islámica. "VIIe Congrès Inernational sur la Céramique Mëdieval en Méditerranée. 11-16 Octobre 1999, Thessaloniki, Greece.

Gómez-Martínez, S., 2005. Cerámica a molde de época islámica. Arqueologia Medieval 9, 221–232.

Gómez-Martínez, S., 2006, La cerámica islámica de Mértola producción y comercio [Tesis de la Universidad Complutense de Madrid] Institutional Repository of the Complutense University of Madrid: https://docta.ucm.es/entities/publication/a727dbc3-755b-457a-ad49-6af169c0f151.

Gómez Martínez, S., 2014. La cerámica islámica de mértola. Campo Arqueológico de Mértola.

Gómez Martínez, S., 2016. El arrabal portuario de *Mértola* (Portugal): El registro cerámico andalusí. Onoba. Revista De Arqueología y Antigüedad 4, 181–196.

Gómez Moreno Martínez, M., 1924. Cerámica medieval española, Barcelona.

Gómez Moreno Martínez, M., 1940. La loza primitiva de Málaga. Al-Andalus 5, 383–398.

Gutierrez, P.C., Pradell, T., Molera, J., Smith, A.D., Climent-Font, A., Tite, M.S., 2010. Color and golden shine of silver Islamic luster. J. Am. Ceram. Soc. 93 (8), 2320–2328. https://doi.org/10.1111/j.1551-2916.2010.03741.x.

Heidenreich, A., 2012. La loza dorada temprana en el ámbito mediterráneo y la implementación de la nueva técnica en la Península Ibérica – una aproximación. In Patronato de la Alhambra y Generalife (Ed.), Actas del I Congreso Red Europea de Museos de Arte Islámico (REMAI) (pp. 271–297). Patronato de la Alhambra y Generalife.

Heimann, R.B., Maggetti, M., 1981. Experiments on simulated burial of calcareous terra sigillata (mineralogical change). Scientific Studies in Ancient Ceramics 19, 163–177.

Heimann, R.B., Maggetti, M., 2019. The struggle between thermodynamics and kinetics: Phase evolution of ancient and historical ceramics. In: Mineralogical Society of Great Britain and Ireland eBooks, pp. 233–282, doi: 10.1180/emu-notes.20.6.

Holakooei, P., De Lapérouse, J., Carò, F., Röhrs, S., Franke, U., Müller-Wiener, M., Reiche, I., 2019. Non-invasive scientific studies on the provenance and technology of early Islamic ceramics from Afrasiyab and Nishapur. J. Archaeol. Sci. Rep. 24, 759–772. https://doi.org/10.1016/j.jasrep.2019.02.029.

Martínez Cabiró, B., 1975. Sobre la loza primitiva de reflejo metálico. Archivo Español de Arte 48, 57–82.

Mason, R.B., 2004. Shine like the sun. Lustre-painted and associated pottery from the Medieval Middle East. In: Bibliotheca Iranica: Islamic art and architecture series, vol 12. Mazda Publishers, Inc.

Mason, R.B., Tite, M.S., 1997. The beginnings of tin-opacification of pottery glazes. Archaeometry 39 (1), 41–58. https://doi.org/10.1111/j.1475-4754.1997.tb00789.x.

Matin, M., 2018. Tin-based opacifiers in archaeological glass and ceramic glazes: a review and new perspectives. Archaeol. Anthropol. Sci. 11 (4), 1155–1167. https://doi.org/10.1007/s12520-018-0735-2.

Matin, M., Tite, M., Watson, O., 2018. On the origins of tin-opacified ceramic glazes: new evidence from early Islamic Egypt, the Levant, Mesopotamia, Iran, and Central Asia. J. Archaeol. Sci. 97, 42–66. https://doi.org/10.1016/j.jas.2018.06.011.

Molera, J., Pradell, T., Salvadó, N., Vendrell-Saz, M., 2001. Interactions between clay bodies and lead glazes. J. Am. Ceram. Soc. 84 (5), 1120–1128. https://doi.org/10.1111/j.1151-2916.2001.tb00799.x.

Molera, J., Bayés, C., Roura, P., Crespo, D., Pradell, T., 2007. Key parameters in the production of medieval luster colours and shines. J. Am. Ceram. Soc. 90 (7), 2245–2254. https://doi.org/10.1111/j.1551-2916.2007.01563.x.

Molera, J., Coll, J., Labrador, A., Pradell, T., 2013. Manganese brown decorations in 10th to 18th century Spanish tin glazed ceramics. Appl. Clay Sci. 82, 86–90. https://doi.org/10.1016/j.clay.2013.05.018.

Molera, J., Carvajal López, J.C., Molina, G., Pradell, T., 2018. Glazes, colourants and decorations in early Islamic glazed ceramics from the vega of Granada (9th to 12th centuries CE). J. Archaeol. Sci. Rep. 21, 1141–1151. https://doi.org/10.1016/j.jasrep.2017.05.017.

Molera, J., Ferreras, V.M., Fusaro, A., Esparraguera, J.M.G., Gaudenzi, M., Pidaev, S.R., Pradell, T., 2019. Islamic glazed wares from ancient Termez (southern Uzbekistan). Raw materials and techniques. J. Archaeol. Sci. Rep. 29, 102169. https://doi.org/10.1016/j.jasrep.2019.102169.

Nodari, L., Marcuz, E., Maritan, L., Mazzoli, C., Russo, U., 2007. Hematite nucleation and growth in the firing of carbonate-rich clay for pottery production. J. Eur. Ceram. Soc. 27 (16), 4665–4673. https://doi.org/10.1016/j.jeurceramsoc.2007.03.031.

Oliveira, J., Silva, J., 1990. *Carta geológica de Portugal à escala 1:50 000*, Folha 46-D, Mértola. Serviços Geológicos de Portugal.

Oliveira, J.T., Silva, J.B., 2007. Geological Map of Portugal, scale 1:500000, with esplicative notes. Map, 46-D/Mértola.

Ouahabi, M.E., Daoudi, L., Hatert, F., Fagel, N., 2015. Modified mineral phases during clay ceramic firing. Clay Clay Miner. 63 (5), 404–413. https://doi.org/10.1346/ccmn.2015.0630506.

Paixão, A., Carvalho, R., Faria. J.C., 2001. Contributo para o estudo da ocupaçãomuçulmana no castelo de Alcácer do Sal: o Convento de Aracoelli. Arqueologia Medieval. Porto: Edições Afrontamento. ISSN 0872-2250. n° 7. pp. 197-209.

Pradell, T., 2016. Lustre and Nanostructures—Ancient Technologies revisited. In: Atlantis Press eBooks, pp. 3–39, DOI: 10.2991/978-94-6239-198-7_1.

Pradell, T., Molera, J., 2020. Ceramic technology. How to characterise ceramic glazes. Archaeol. Anthropol. Sci. 12 (8). https://doi.org/10.1007/s12520-020-01136-9.

Pradell, T., Molera, J., Smith, A., Tite, 2007. The invention of lustre: Iraq 9th and 10th centuries AD. J. Archaeol. Sci. 35(5), 1201–1215. DOI: 10.1016/j.jas.2007.08.016.

Pradell, T., Molera, J., Smith, A., Tite, 2008a. Early Islamic lustre from Egypt, Syria and Iran (10th to 13th century AD). J. Archaeol. Sci. 35(9), 2649–2662, Doi: 10.1016/j.jas.2008.05.011.

Pradell, T., Molera, J., Smith, A.D., Climent-Font, A., Tite, M.S., 2008b. Technology of Islamic lustre. J. Cult. Herit. 9, e123–e128. https://doi.org/10.1016/j.culher.2008.06.010.

Pradell, T., Molera, J., Smith, A.D., Tite, M.S., 2008c. The invention of lustre: Iraq 9th and 10th centuries AD. J. Archaeol. Sci. 35 (5), 1201–1215. https://doi.org/10.1016/j.jas.2007.08.016.

Pradell, T., Molera, J., Molina, G., Tite, 2013. Analysis of Syrian lustre pottery (12th–14th centuries AD). Appl. Clay Sci., 82, 106–112. DOI: 10.1016/j.clay.2013.05.019.

Quinn, P.S., 2013. Ceramic petrography: the interpretation of archaeological pottery & related artefacts in thin section. DOI: 10.2307/j.ctv1jk0jf4.

Rathossi, C., Pontikes, Y., Tsolis-Katagas, P., 2017. Mineralogical differences between ancient sherds and experimental ceramics: Indices for firing conditions and post-burial alteration. Bull. Geol. Soc. Greece 43 (2), 856. https://doi.org/10.12681/bgsg.11251.

Riccardi, M., 1999. An approach to the dynamics of clay firing. Appl. Clay Sci. 15 (3–4), 393–409. https://doi.org/10.1016/s0169-1317(99)00032-0.

Rosser-Owen, M., 2012. From the mounds of Old Cairo": Spanish ceramics from Fustat in the collections of the Victoria and Albert Museum. In Patronato de la Alhambra y Generalife (Ed.), Actas del I Congreso Red Europea de Museos de Arte Islámico (REMAI) (pp. 163–187).

Salinas, E., Pradell, T., 2020a. The introduction of the glaze in al-Andalus: Technological waves and oriental influences. Libyan Studies 51, 87–98. https://doi.org/10.1017/lis.2020.8.

Salinas, E., Pradell, T., 2020b. Madīnat al-Zahrā' or Madīnat Qurtuba? first evidences of the Caliphate tin glaze production of 'verde y manganeso' ware. Archaeol. Anthropol. Sci. 12 (9). https://doi.org/10.1007/s12520-020-01170-7.

Salinas, E., Pradell, T., 2024. The secret is quartz: technology of production of an eleventh-twelfth century western Mediterranean polychrome glazed ware. Archaeol. Anthropol. Sci. 16 (8). https://doi.org/10.1007/s12520-024-02040-2.

Salinas, E., Pradell, T., Tite, M., 2017. Tracing the tin-opacified yellow glazed ceramics in the western Islamic world: the findings at Madīnat al-Zahrā'. Archaeol. Anthropol. Sci. 11 (3), 777–787. https://doi.org/10.1007/s12520-017-0562-x.

Salinas, E., Pradell, T., Molera, J., 2018b. Glaze production at an early Islamic workshop in al-Andalus. Archaeol. Anthropol. Sci. 11 (5), 2201–2213. https://doi.org/10.1007/s12520-018-0666-y.

Scanlon, G.T., 1998. Slip-painted early lead-glazed wares from Fustat: A dilemma of nomenclature. In R. P. Gayraud (Ed.), Colloque international d'Archéologie Islamique, 3–7 février 1993 (pp. 21–53). Cairo: Institut Français d'Archéologie Orientale (IFAO).

Schermerhorn, L., 1971. An outline stratigraphy of the Iberian Pyrite Belt. Boletim Geológico Mineiro 82, 239–268.

Schiavon, N., Soria, V., Arruda, A.M., Beltrame, M., Mirão, J., 2015. "Losanga" decorated imitations of italic late republican black gloss tableware from South-Western Iberia: a multi-analytical/microchemical characterization. Microchem. J. 124, 712–718. https://doi.org/10.1016/j.microc.2015.10.017.

Taxel, I., 2014. Luxury and common wares: socio-economic aspects of the distribution of glazed pottery in Early Islamic Palestine. Levant 46 (1), 118–139. https://doi.org/10.1179/0075891413z.00000000036.

Ting, C., Taxel, I., Merkel, S.W., Tal, O., 2025. The glaze is less opaque on the other side: the development of Egyptian and southern Levantine glazed ceramic production from the early Islamic to Crusader periods. J. Archaeol. Sci. 179, 106255. https://doi.org/10.1016/j.jas.2025.106255.

Tite, M.S., Freestone, I., Mason, R., Molera, J., Vendrell-saz, M., Wood, N., 1998. Lead Glazes in Antiquity—Methods of production and reasons for use. Archaeometry 40 (2), 241–260. https://doi.org/10.1111/j.1475-4754.1998.tb00836.x.

Tite, M., Watson, O., Pradell, T., Matin, M., Molina, G., Domoney, K., Bouquillon, A., 2015. Revisiting the beginnings of tin-opacified Islamic glazes. J. Archaeol. Sci. 57, 80–91. https://doi.org/10.1016/j.jas.2015.02.005.

Walton, M.S., Tite, M.S., 2010. Production technology of Roman lead-glazed pottery and its continuance into late antiquity. Archaeometry 52 (5), 733–759. https://doi.org/10.1111/j.1475-4754.2009.00506.x.

Watson, O., 1985. *Persian Lustre Ware*. Faber and Faber.

Watson, O., 2014. Revisiting Samarra: the rise of Islamic glazed pottery. Beiträge Zur Islamischen Kunst Und Archäologie 4, 123–142.

Wentworth, C.K., 1922. A scale of grade and class terms for clastic sediments. J. Geol. 30 (5), 377–392. http://www.jstor.org/stable/30063207.

Whitcomb, D., 1989. Coptic glazed ceramics from the excavations at Aqaba, Jordan. J. Am. Res. Center in Egypt 26, 167. https://doi.org/10.2307/40000705.

Wood, N., Tite, M.S., Doherty, C., Gilmore, B., 2007. A technological examination of ninth–tenth century ad abbasid blue-and-white ware from Iraq, and its comparison with eighth century ad Chinese blue-and-white Sancai ware*. Archaeometry 49 (4), 665–684. https://doi.org/10.1111/j.1475-4754.2007.00327.x.

Zhao, B., 2013. Luxury and power: the fascination with chinese ceramics in medieval Swahili material culture. Orientations 44 (4), 71–78.

Zozaya J., Aparicio, A., 2003. Análisis de cerámicas andalusíes. "VIIe Congrès Inernational sur la Céramique Mëdieval en Méditerranée. 11-16 Octobre 1999, Thessaloniki, Greece.

Zozaya, J., Retuerce, M., Aparicio, A., 1995. Cerámica andalusí de reflejo dorado: 1195-1212. Actes De 5éme Colloque Sur La Céramique Médiévale [Mediterranéene]. 11-17 Novembre 1991, Rabat, Morocco.